

Unsupervised Anomaly Detection in Multivariate Time Series across Heterogeneous Domains

Vincent Jacob
Ecole Polytechnique
Palaiseau, France
vincent.jacob@polytechnique.edu

Yanlei Diao
Ecole Polytechnique
Palaiseau, France
yanlei.diao@polytechnique.edu

ABSTRACT

The widespread adoption of digital services, along with the scale and complexity at which they operate, has made incidents in IT operations increasingly more likely, diverse, and impactful. This has led to the rapid development of a central aspect of “Artificial Intelligence for IT Operations” (AIOps), focusing on detecting anomalies in vast amounts of multivariate time series data generated by service entities. In this paper, we begin by introducing a unifying framework for benchmarking unsupervised anomaly detection (AD) methods, and highlight the problem of shifts in normal behaviors that can occur in practical AIOps scenarios. To tackle anomaly detection under domain shift, we then cast the problem in the framework of domain generalization and propose a novel approach, Domain-Invariant VAE for Anomaly Detection (DIVAD), to learn domain-invariant representations for unsupervised anomaly detection. Our evaluation results using the Exathlon benchmark show that the two main DIVAD variants significantly outperform the best unsupervised AD method in maximum performance, with 20% and 15% improvements in maximum peak F1-scores, respectively. Evaluation using the Application Server Dataset further demonstrates the broader applicability of our domain generalization methods.

1 INTRODUCTION

Time series anomaly detection has been studied intensively due to its broad application to domains such as financial market analysis, system diagnosis, and mechanical systems [11, 19]. Recently, it has been increasingly adopted in an emerging domain known as “Artificial Intelligence for IT operations” (AIOps) [17], which proposes to use AI to automate and optimize large-scale IT operations [58]. Not long ago, the role of IT was to support the business. Today as digital services and applications become the primary way that enterprises serve and interact with customers, IT *is* the business – almost every business depends on the continuous performance and innovation of its digital services.

With this paradigm shift, incidents in IT operations have become more impactful, inducing ever-increasing financial costs, both directly through service-level agreements made with customers and indirectly through brand image deterioration. Concurrently, the popularity of such services, along with their widespread migration to the cloud, has greatly increased the scale and complexity at which they operate, relying on more resources to process larger volumes of data at high speed. This evolution has made incidents more frequent, costly, diverse, and difficult for engineers to manually anticipate and diagnose, thus calling for more automated solutions.

To respond to such needs, this paper focuses on *anomaly detection in multivariate time series* that suits the challenges in AIOps.

More specifically, a large set of multivariate time series are generated from the periodic monitoring of service entities, and “anomalies” are reported as patterns in data that deviate from a given notion of *normal behavior* [10].

Challenges. Detecting anomalies in AIOps presents a set of technical challenges [58]. (CH1) The *scarcity of anomaly labels* is due to the lack of domain knowledge of IT operations to reliably label anomalies, and the labor-intensive process of examining large amounts of time series data. (CH2) The *high dimensionality of recorded time series*, both in terms of time and feature dimensions, is common in AIOps due to the collection of numerous metrics at high frequency across a large number of entities. (CH3) The *complexity and variety in normal behaviors* arise because multiple, complex entities are monitored at scale in different contexts. (CH4) The *shifts in normal behaviors* further arise due to potentially frequent changes in software/service components, hardware components, or operation contexts of the monitored entities. The recent Exathlon benchmark [25] exhibits significant shifts in normal behaviors across traces collected from different runs of Spark streaming applications. Similarly, the Application Server Dataset (ASD) [30] exhibits shifts in behaviors of different servers. In these cases, the shifts in normal behaviors are so significant that they appear to be samples collected from different *domains* or *contexts*.

A large number of anomaly detection (AD) methods for multivariate time series have been developed, as categorized recently by Schmidl et al. [45]. CH1 has been typically addressed through the development of *unsupervised* AD methods, assuming no label information for training, and *semi-supervised* methods that assume (possibly noisy) labels for the normal class only [10]. In this paper, we jointly refer to them as “unsupervised” methods, trained on mostly-normal data and evaluated on a labeled test set. Concurrently, the advent of *deep learning* (DL) [28] has been instrumental in partly addressing CH2 and CH3, offering the ability to learn succinct yet effective representations of high-dimensional data while capturing both temporal (i.e., intra-feature) and spatial (i.e., inter-feature) dependencies in multivariate time series [30, 50, 57]. Despite covering a wide range of assumptions about both normal data and anomalies, all these methods are vulnerable to CH4, by assuming a similar distribution of training and test normal data, which makes them of limited use in the new AIOps scenario.

This paper tackles the last challenge (CH4), compounded by other challenges (CH1-Ch3), through the framework of **domain generalization** (DG). In this framework, data samples are collected from multiple, distinct *domains* (the normal contexts here), with certain characteristics of the observed data being determined by the domain, and others being independent from it. This amounts to associating shifts in normal behavior to the concept of *domain*

shift, and aiming to build models from a set of training (or *source*) domains that can generalize to another set of test (or *target*) domains. Most of existing DG methods were proposed for image classification, categorized as based on *explicit feature alignment*, *domain-adversarial learning* or *feature disentanglement* [53, 60]. In practice, adversarial methods can suffer from instabilities that make them hard to reproduce [27, 41], and explicit feature alignment become very costly as the number of source domains increases, like in AIOps. For these reasons, this paper focuses on feature disentanglement [24, 37, 38], where methods seek to decompose the input data into *domain-shared* and *domain-invariant* features. The existing methods, designed for image classification, are not applicable to unsupervised time series anomaly detection (with no labels). Further, recent efforts on domain generalization for time series AD handle only univariate sound waves with various labeling assumptions [13], making them unsuitable for the AIOps setting.

Contributions. In this paper, we present the first *multivariate time series anomaly detection approach that generalizes across heterogeneous domains*. Given that this topic has been underaddressed in the anomaly detection literature, we conduct an in-depth study to characterize the problem of normal behavior shifts using the recent Exathlon benchmark [25] (which was motivated by AIOps use cases) and to highlight the performance issues of existing unsupervised anomaly detection methods under domain shift. We then address this challenge by proposing a novel approach based on domain generalization and feature disentanglement, custom-designed for unsupervised time series anomaly detection. More specifically, our paper makes the following contributions:

- We introduce a unifying framework for benchmarking unsupervised anomaly detection methods, and highlight the domain shift problem in AIOps scenarios (Section 3).
- To tackle the problem of domain shift, we develop a theoretical formulation of unsupervised anomaly detection in the framework of *domain generalization* (Section 4).
- In this proposed framework, we develop a novel approach, called Domain-Invariant VAE for Anomaly Detection (DIVAD), with a set of variants to learn domain-invariant representations, thereby enabling effective anomaly detection in unseen domains (Section 5).

Our evaluation using the Exathlon benchmark shows that our two main DIVAD variants can significantly outperform the best unsupervised AD method in maximum performance, with 20% and 15% improvements in maximum peak F1-scores (0.79 and 0.76 over 0.66), respectively. Our evaluation also applies DIVAD to the Application Server Dataset (ASD) [30], reflecting a similar use case, and shows that its explicit domain generalization can be more broadly applicable and useful in this second use case.

The code for our DIVAD method and experiments is available at <https://github.com/exathlonbenchmark/divad>.

2 RELATED WORK

Anomaly Detection in Multivariate Time Series. Numerous unsupervised anomaly detection methods in multivariate time series have been proposed over the years [10, 11, 19]. Schmidl et al. [45] recently introduced a taxonomy based on the way the methods derive their *anomaly scores* for data samples (the higher the score,

the more deemed anomalous by the method). The only category we do not consider in this work is *distance methods*, which typically do not scale well with the large dimensionality of AIOps.

Forecasting methods define anomaly scores of data samples as forecasting errors, based on the distance between the forecast and actual value(s) of one or multiple data point(s) in a context window of length L . LSTM-AD [34] is the most popular forecasting method. It trains a stacked LSTM network to predict the next l data records from the first $L - l$ of a window. It then fits a multivariate Gaussian distribution to the error vectors it produced in a validation set, and defines the anomaly score of a record as the negative log-likelihood of its error with respect to this distribution.

Reconstruction methods score data samples based on their reconstruction errors from a transformed space. Principal Component Analysis (PCA) [3] and Autoencoder (AE) [21, 44] are representative shallow and deep reconstruction methods, respectively. PCA’s transformation is a projection on the linear hyperplane formed by the principal components of the data, while AE’s is a non-linear mapping to a latent encoding learned by a neural network that was trained to reconstruct data from it. More recently, Multi-Scale Convolutional Recurrent Encoder-Decoder (MSCRED) [57] turns a multivariate time series into multi-scale signature matrices characterizing system status at different time steps, and learns to reconstruct them using convolutional encoder-decoder and attention-based ConvLSTM networks. TranAD [50] relies on two transformer-based encoder-decoder networks, with the first encoder considering the current input window, and the second one considering a larger *context* of past data in the window’s sequence. It defines the anomaly score of an input window as the average of its reconstruction errors coming from two decoders and inference phases, with the second phase using the reconstruction error from the first phase as a focus score to detect anomalies at a finer level.

Encoding methods score data samples based on their deviation within a transformed space. Deep SVDD [42] is the most popular recent encoding method, training a neural network to map the input data to a latent representation enclosed in a small hypersphere, and defining anomaly scores of test samples as their squared distance from this hypersphere’s centroid. More recently, DCDetector [56] uses a dual-view attention structure based on contrastive learning to derive representations where differences between normal points and anomalies are amplified, subdividing windows into adjacent “patches”, with one view modeling relationships within patches and the other across patches. To derive anomaly scores, it uses the insight that normal points tend to be similarly correlated for both views, while anomalies tend to be more correlated to their adjacent points than to the rest of the window.

Distribution methods define anomaly scores of data samples as their deviation from an estimated distribution of the data. The Mahalanobis method [3, 47] and Variational Autoencoder (VAE) [7] are representative shallow and deep distribution methods, respectively. The Mahalanobis method estimates the data distribution as a multivariate Gaussian, and defines the anomaly score of a test vector as its squared Mahalanobis distance from it. VAE estimates it using a variational autoencoder, with the anomaly score of a test point derived by drawing multiple samples from its probabilistic encoder, and averaging the negative log-likelihood of the reconstructions obtained from each of these samples. A more recent method is

OmniAnomaly [48]. It estimates the distribution of multivariate windows with a stochastic recurrent neural network, explicitly modeling temporal dependencies among variables through a combination of GRU and VAE. It then defines a test window’s anomaly score as the negative log-likelihood of its reconstruction.

Isolation tree methods score data samples based on their “isolation level” from the rest of the data. Isolation forest [31] is the most popular isolation tree method. It trains an ensemble of trees to isolate the samples in the training data, and defines the anomaly score of a test instance as inversely proportional to the average path length required to reach it using the trees.

Overall, these methods cover a wide range of assumptions about both normal data and anomalies. As we show in this paper, *by assuming a similar distribution of training and test normal data, all of them are vulnerable to shifts in normal behavior*, limiting their applicability in our AIOps scenario.

Domain Generalization. Domain generalization (DG) has been mainly studied in the context of *image classification*, with the domains usually corresponding to the way images are represented or drawn. DG methods can broadly be categorized as based on *explicit feature alignment*, *domain-adversarial learning* or *feature disentanglement* [53, 60]. Explicit feature alignment methods seek to learn data representations where feature distribution divergence is explicitly minimized across domains, with divergence metrics including the Wasserstein distance or Kullback-Leibler divergence [53, 60]. Rather than using such divergence metrics directly, domain-adversarial learning methods seek to minimize domain distribution discrepancy through a minimax two-player game, where the goal is to make the features confuse a domain discriminator [16], usually implemented as a domain classifier [4, 29, 35, 46]. Such adversarial methods can suffer from instabilities that make them hard to reproduce [27, 41], while explicit feature alignment can become very costly as the number of source domains increases, like in AIOps. For these reasons, this work considers domain generalization based on feature disentanglement [24, 37, 38], where methods seek to decompose the input data into *domain-specific* and *domain-invariant* features, and perform their tasks in domain-invariant space.

Our work is specifically related to Domain-Invariant Variational Autoencoders (DIVA) [24], designed for image classification. It uses variational autoencoders (VAE) to decompose input data into domain-specific, class-specific, and residual latent factors, conditioning the distributions of its domain-specific and class-specific factors on the training domain and class, respectively, and enforcing this conditioning by using classification heads to predict the domain and class from the corresponding embeddings. It then uses its class-related classifier to derive its predictions for the test images. Because of this class supervision, this method cannot be applied to our unsupervised AD setting.

Domain generalization for time series AD recently gained attention through anomalous sound detection and the DCASE2022 Challenge, where the task was to identify whether a machine was normal or anomalous using only normal sound data under domain-shifted conditions [13]. The methods proposed however modeled single-channel (univariate) sound waves, while also assuming labels such as the machine state, the type of machine, domain shift or noise

considered to train domain-invariant or disentangled representations [52]. This univariate aspect, coupled with these simplifying assumptions, makes such methods unsuitable for our AIOps setting.

Data Drift Detection. Many techniques exist for data drift detection [15]. However, popular methods such as using the Kolmogorov-Smirnov distance [9, 14] require a significant amount of drifted data to detect a distribution change accurately. Anomaly detection under domain shift is essentially a different problem, where anomalies must be detected with low latency as they arise, although the normal behaviors in the current domain may appear to be drawn from a different context from those seen in training data.

3 GENERAL AD FRAMEWORK

In this section, we present the unsupervised anomaly detection (AD) problem, propose a unifying framework to encompass AD approaches in evaluation, and highlight the presence of domain shift in the current framework using the Exathlon [25] benchmark.

3.1 Unsupervised Anomaly Detection

We first introduce the notation of the paper and define the AD problem in the unsupervised setting. More specifically, we consider N_1 training sequences and N_2 test sequences:

$$\mathcal{S}_{\text{train}} = (\mathcal{S}^{(1)}, \dots, \mathcal{S}^{(N_1)}), \quad \mathcal{S}_{\text{test}} = (\mathcal{S}^{(N_1+1)}, \dots, \mathcal{S}^{(N_1+N_2)}),$$

where each $\mathcal{S}^{(i)}$ consists of T ordered data records of dimension M . To simplify the notation, our problem definition uses T to denote the (same) length of all sequences, while our techniques do not make this assumption and can handle variable-length sequences.

For each *test* sequence, we consider a sequence of *anomaly labels*:

$$\mathcal{Y}_{\text{test}} = \{\mathbf{y}^{(N_1+1)}, \dots, \mathbf{y}^{(N_1+N_2)}\},$$

with $\mathbf{y}^{(i)} \in \{0, 1\}^T$, such that:

$$\begin{cases} y_t^{(i)} = 1 & \text{if the record at index } t \text{ in sequence } i \text{ is } \textit{anomalous}, \\ y_t^{(i)} = 0 & \text{otherwise (i.e., the record is } \textit{normal}). \end{cases}$$

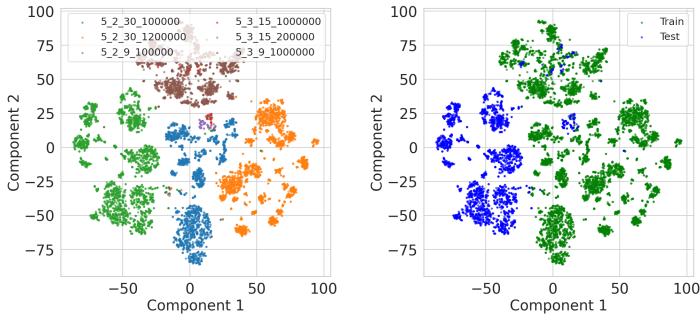
Our goal is to build an anomaly detection model as follows.

DEFINITION 1. *An anomaly detection model is a record scoring function $g : \mathbb{R}^{T \times M} \rightarrow \mathbb{R}^T$, mapping a sequence S to a sequence of real-valued record-wise anomaly scores $g(S)$, which assigns higher anomaly scores to anomalous records than to normal records in test sequences. That is, $g(S^{(i)})_{t_1} > g(S^{(j)})_{t_2}, \forall i, j \in [N_1 \dots N_1 + N_2], t_1, t_2 \in [1 \dots T]$ s.t. $y_{t_1}^{(i)} = 1 \wedge y_{t_2}^{(j)} = 0$.*

This record scoring function should further be constructed in a setting of *offline training* and *online inference*. More precisely, it means that training has to be performed offline on $\mathcal{S}_{\text{train}}$, and inference must be performed online on $\mathcal{S}_{\text{test}}$ by considering only the data preceding a given record at time index t :

$$g(S^{(i)})_t = g(S_{1:t}^{(i)})_t, \quad \forall i \in [N_1 \dots N_1 + N_2], \quad t \in [1 \dots T].$$

Due to this requirement, we refer to the anomaly detection methods based on g as *online scorers*.



(a) Records colored by context. (b) Records colored by dataset.

Figure 1: t-SNE scatter plots of application 2’s normal data, under-sampled to 10,000 data records balanced by context.

3.2 Unifying Anomaly Detection Framework

We next propose a unifying framework to encompass AD approaches within a common evaluation structure. In this framework, each online scorer relies on a *windowing operator* W_L that extracts sliding windows, or *samples*, of length $L > 0$ from a given sequence i :

$$W_L(S^{(i)}) = \{S_{t-L+1:t}^{(i)}\}_{t=L}^T =: \{x_t^{(i)}\}_{t=L}^T,$$

with $x_t^{(i)} \in \mathbb{R}^{L \times M}$. Then the training set is composed of the samples extracted from all the training sequences:

$$\mathcal{D}_{\text{train}} := \bigcup_{i \in [1..N_1]} \{W_L(S^{(i)})\}.$$

DEFINITION 2. A window scorer, trained on $\mathcal{D}_{\text{train}}$, is a window scoring function that assigns an anomaly score to a given window, proportional to its abnormality for the method, $g_W : \mathbb{R}^{L \times M} \rightarrow \mathbb{R}$, $x \mapsto g_W(x)$.

We encapsulate each individual AD method within a window scorer, and then propose a universal *online scorer* constructed from the window scorer. Given a test sequence S and a smoothing factor $\gamma \in [0, 1)$, the online scorer assigns anomaly scores as follows:

$$g(S; L, \gamma)_t = \begin{cases} -\infty & \text{if } t < L, \\ (1 - \gamma)\hat{y}_t =: m_L & \text{if } t = L, \\ \frac{\gamma m_{t-1} + (1 - \gamma)\hat{y}_t}{(1 - \gamma^{t+1})} =: m_t & \text{if } t > L. \end{cases}$$

With:

$$\hat{y}_t = g_W(S_{t-L+1:t}), \forall t \in [L..T].$$

In other words, for a test sequence, we assign an anomaly score to the current sliding window of length L using g_W (which is fixed and trained offline). We then define this window score as the anomaly score of its last record (i.e., the one just received in an online setting). To allow additional control on the tradeoff between the “stability” and “reactivity” of the record scoring function¹, we further apply an *exponentially weighted moving average* with smoothing hyperparameter γ to the anomaly scores. This produces the final output of the record scoring function g for a test sequence, prepended with infinitely low anomaly scores for the timestamps before its first full window of length L . In this framework, both L and γ are hyperparameters to set for every anomaly detection method.

¹This tradeoff is also influenced by the window length L , the window scoring function and the types of anomalies.

3.3 Domain Shift in Exathlon

Inspired by real-world AIOps use cases, the Exathlon benchmark [25] is one of the most challenging benchmarks for anomaly detection due to the high-dimensionality and complex, diverse behaviors in its dataset, as reported in a recent comprehensive experimental study of AD methods [45].

3.3.1 *Background on Exathlon.* Exathlon [25] has been systematically constructed based on repeated executions of distributed Spark streaming *applications* in a cluster under different Spark *settings* and *input rates*. The dataset includes 93 repeated executions of 10 Spark applications, with one *trace* collected for each execution containing 2,283 raw features, resulting in a total size of 24.6GB. While 59 traces were collected in normal execution (*normal traces*), 34 other traces were disturbed manually by injecting anomalous events (*disturbed traces*). There are 6 different classes of anomalous events (e.g., misbehaving inputs, resource contention, process failures), with a total of 97 anomalous instances. For each of these anomalies, Exathlon provides the ground truth label for the interval spanning the root cause event and its lasting effect, enabling accurate evaluation of AD methods. In addition to anomalous instances, both the normal and disturbed traces contain enough variety (e.g., Spark’s checkpointing activities) to capture diverse normal behaviors.

3.3.2 *Analysis of Domain Shift.* Given the limited number of Spark *applications* (or *entities* [59]) in the Exathlon dataset, our study focuses on the ability of an AD method to generalize, not to new applications, but rather to the new *contexts* of the Spark applications. For this reason, the **domain** of a trace is defined as its *context*, characterized by the following factors: (i) The Spark *settings* for each application run includes its processing period (i.e., batch interval or window slide), set to a specific value for the application, the number of active executors and “memory profile” (i.e., maximum memory set for the driver block manager, executors JVM, and garbage collection). The last two aspects had either a direct or indirect impact on a lot of features (e.g., executors memory usage). (ii) The *input rate* is the rate at which data records were sent to the application, which had a direct effect on many recorded features (e.g., last completed batch processing delay). The “normal behavior” in a trace is, therefore, mainly determined by its trace characteristics, defined as the combination of its *entity* and *domain/context*.

To illustrate the *diversity* and *shift* in domains/contexts, Figure 1 shows t-SNE scatter plots [51] of application 2’s normal data, under-sampled to 10,000 data records. The *diversity* is shown in Figure 1a, where data records are colored by context (where context labels include the processing period, number of Spark executors, maximum executors memory, and data input rate). We see that different contexts appear as distinct clusters, constituting a *multimodal* distribution for data records. Figure 1b illustrates the *shift* in context: the different contexts induce a distribution shift from the training to the test data, even within normal records of the same application—we refer to this phenomenon as the *domain shift* problem.

4 PROBLEM OF DOMAIN SHIFT

In this section, we formally define the problem of anomaly detection under domain shift. We took inspiration from one of the first adopted definitions of an *anomaly* proposed by Douglas M.

Hawkins in 1980, describing it as “an observation which deviates so much from the other observations as to arouse suspicions that it was generated by a different mechanism” [20].

This definition naturally suggests addressing our AD problem from a *generative* perspective, assuming data samples were generated from a distribution $p_{\text{data}}(\mathbf{x}, y)^2$, with *normal* samples generated from $p_{\text{data}}(\mathbf{x}|y = 0)$. Our general goal then translates to constructing a **model** $p_{\theta}(\mathbf{x})$ of $p_{\text{data}}(\mathbf{x}|y = 0)$, parameterized by $\theta \in \Theta$. This yields a natural definition for the **anomaly score** of a test sample, as its negative log-likelihood with respect to this model:

$$g_W(\mathbf{x}; \theta) := -\log p_{\theta}(\mathbf{x} = \mathbf{x})$$

Since normal samples from the training and test sets are assumed generated from $p_{\text{data}}(\mathbf{x}|y = 0) \approx p_{\theta}(\mathbf{x})$, we would indeed expect them to have a higher likelihood under this model than anomalous samples, generated from $p_{\text{data}}(\mathbf{x}|y = 1) \neq p_{\theta}(\mathbf{x})$.

A unique aspect of AIOps scenarios, however, is that the distribution generating an observed sample can be conditioned not only on its class, but also on the specific *sequence* this sample was extracted from. In particular, each sequence corresponds to a **domain/context** that impacts the distribution of observed data, even for the same entity being recorded. These domains can be included in our generative model, by assuming that the selection of a sequence i corresponds to the realization d_i of a discrete random domain variable $d \sim p_{\text{data}}(d)$ with infinite support³. In this setting, the samples of class $c \in \{0, 1\}$ from sequence i can be seen as independently drawn from a sequence-induced, or *domain* distribution:

$$p_i(\mathbf{x}|y = c) = p_{\text{data}}(\mathbf{x}|y = c, d = d_i).$$

This amounts to assuming the distribution of \mathbf{x} is conditioned on the two independent variables d and y , the former determining the domain the sample originates from, and the latter determining whether the sample is normal or anomalous. We illustrate the corresponding generative model in Figure 2a. Under this model, the data-generating distribution of normal samples can be expressed as the countable mixture of all possible domain distributions:

$$p_{\text{data}}(\mathbf{x}|y = 0) = \sum_{d=1}^{\infty} p_{\text{data}}(\mathbf{x}|y = 0, d = d)p_{\text{data}}(d = d).$$

DEFINITION 3 (DOMAIN SHIFT CHALLENGE). *Directly applying traditional generative methods in an unsupervised setting amounts to making $p_{\theta}(\mathbf{x})$ estimate the data-generating distribution of the normal training samples (with d_i ’s fixed and all samples equally-likely to come from every sequence i):*

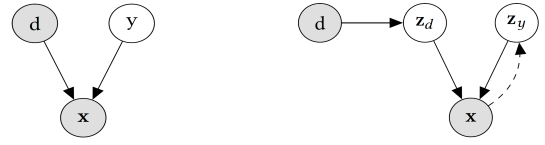
$$p_{\text{train}}(\mathbf{x}|y = 0) = \frac{1}{N_1} \sum_{i=1}^{N_1} p_{\text{data}}(\mathbf{x}|y = 0, d = d_i),$$

which, given the infinitude of possible domains, is likely to differ from the data-generating distribution of the normal test samples:

$$p_{\text{test}}(\mathbf{x}|y = 0) = \frac{1}{N_2} \sum_{i=N_1+1}^{N_1+N_2} p_{\text{data}}(\mathbf{x}|y = 0, d = d_i),$$

²To simplify the notation, we use y to refer to the label of an input *sample* in the following: $y = 0$ if the sample is (fully) normal, $y = 1$ otherwise.

³We use d_i (as opposed to i) to reflect the fact that multiple sequences can correspond to the same context, and thus value d (i.e., we can have $d_i = d_j$ for $i \neq j$).



(a) Observed variable \mathbf{x} depends on its domain d and domain-specific z_d and domain-independent (unobserved) class y . (b) \mathbf{x} is caused by independent domain-specific z_d and domain-independent z_y .

Figure 2: Generative models. For (b), constructing f_y amounts to inferring z_y from \mathbf{x} (dashed arrow).

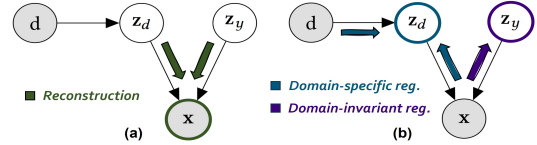


Figure 3: Illustration of the (a) reconstruction and (b) regularization terms in the ELBO objective (Eq. 1).

with $\{d_i\}_{i=1}^{N_1} \neq \{d_i\}_{i=N_1+1}^{N_1+N_2}$. This mismatch induces a domain shift challenge, characterized by test normal samples $\mathbf{x}_0 \sim p_{\text{test}}(\mathbf{x}|y = 0)$ and test anomalous samples $\mathbf{x}_1 \sim p_{\text{test}}(\mathbf{x}|y = 1)$ being both unlikely in uncontrollable ways under $p_{\theta}(\mathbf{x}) \approx p_{\text{train}}(\mathbf{x}|y = 0)$, which hinders anomaly detection performance.

A suitable framework to address this domain shift challenge is *domain generalization* [53, 60]. In this framework, the domains sampled for training are referred to as *source domains*, while those sampled at test time are called *target domains*.

DEFINITION 4 (ANOMALY DETECTION WITH DOMAIN GENERALIZATION). *Our problem can be framed as building an AD model from the source domains that generalizes to the target domains. We do so by assuming that the observed variable \mathbf{x} can be mapped via f_y to a latent representation \mathbf{z}_y , whose distribution is (i) discriminative with respect to the class y (i.e., normal vs. anomalous) and (ii) independent from the domain d . Our goal can be formulated as:*

- Finding such a mapping $f_y(\mathbf{x}) = \mathbf{z}_y$;
- Constructing $p_{\theta}(\mathbf{x})$ to estimate $p_{\text{train}}(f_y(\mathbf{x})|y = 0)$ instead of $p_{\text{train}}(\mathbf{x}|y = 0)$.

Since $f_y(\mathbf{x}) = \mathbf{z}_y$ is independent from d , we then have:

$$\begin{aligned} p_{\text{train}}(\mathbf{z}_y|y = 0) &= \frac{1}{N_1} \sum_{i=1}^{N_1} p(\mathbf{z}_y|y = 0, d = d_i) \\ &= p(\mathbf{z}_y|y = 0) = p_{\text{test}}(\mathbf{z}_y|y = 0), \end{aligned}$$

which means that, under $p_{\theta}(\mathbf{x}) \approx p_{\text{train}}(\mathbf{z}_y|y = 0) = p_{\text{test}}(\mathbf{z}_y|y = 0)$, the **normal test samples \mathbf{x}_0 should be more likely than the test anomalies \mathbf{x}_1** , hence addressing the domain shift challenge.

5 THE DIVAD METHOD

In this section, we introduce a new approach to anomaly detection under domain shift. At a high level, our central assumption is that *anomalies should have a sensible impact on the properties of the input samples that are invariant with respect to the domain*. In an AIOps scenario, this means that, although some aspects of a running

process may vary from domain to domain (e.g., its memory used or processing delay), others typically remain constant and characterize its “normal” behavior (e.g., its scheduling delay, processing delay per input record, or any other Key Performance Indicator (KPI) [59] that behaves similarly across contexts). These domain-invariant, normal-specific characteristics tend to reflect whether the process *functions properly*, while domain-specific characteristics simply manifest *different modes of normal operation*.

To realize this intuition, we propose Domain-Invariant VAE for Anomaly Detection, or DIVAD. This method embodies (i) a new generative model with feature disentanglement to decompose the input data into domain-invariant and domain-specific factors, (ii) an effective training approach in the VAE framework, with a custom training objective for our unique AD model, and (iii) different alternatives for model inference, deriving anomaly scores based on the training distribution of domain-invariant factors only.

5.1 Modeling

Based on the notion of *feature disentanglement* [53, 60], our model assumes that the observed variable \mathbf{x} is caused by two *independent* latent factors \mathbf{z}_d and \mathbf{z}_y : (i) \mathbf{z}_d is conditioned on the observed domain d , and (ii) \mathbf{z}_y is assumed independent from it and can be used to detect anomalies in test samples. The corresponding generative model is shown in Figure 2b. Assuming that the model is parameterized by *model parameters* $\theta \in \Theta$, the marginal likelihood $p_\theta(\mathbf{x}|d)$ can be derived based on the structure of the generative model:

$$\begin{aligned} p_\theta(\mathbf{x}|d) &= \int p_\theta(\mathbf{x}, \mathbf{z}_d, \mathbf{z}_y|d) d\mathbf{z}_d d\mathbf{z}_y \\ &= \int p_\theta(\mathbf{x}|\mathbf{z}_y, \mathbf{z}_d) p_\theta(\mathbf{z}_d|d) p(\mathbf{z}_y) d\mathbf{z}_d d\mathbf{z}_y. \end{aligned}$$

5.2 Model Training

We seek to learn the model parameters of $p_\theta(\mathbf{x}|d)$ through maximum likelihood estimation. Since computing $p_\theta(\mathbf{x}|d)$ directly is intractable, we leverage a variational autoencoder (VAE) **framework** [26, 39], considering *variational parameters* $\phi_d, \phi_y \in \Phi$, and optimizing the following evidence lower bound (ELBO) instead, known to be a lower bound on $p_\theta(\mathbf{x}|d)$ and lead to effective learning of its model parameters:

$$\begin{aligned} \mathcal{L}_{\text{ELBO}}(\mathbf{x}, d; \theta_{yd}, \theta_d, \phi_d, \phi_y) = & \\ \mathbb{E}_{q_{\phi_d}(\mathbf{z}_d|\mathbf{x}) q_{\phi_y}(\mathbf{z}_y|\mathbf{x})} [\log p_{\theta_{yd}}(\mathbf{x}|\mathbf{z}_d, \mathbf{z}_y)] & \quad (1) \\ - \beta D_{\text{KL}}(q_{\phi_y}(\mathbf{z}_y|\mathbf{x}) \| p(\mathbf{z}_y)) - \beta D_{\text{KL}}(q_{\phi_d}(\mathbf{z}_d|\mathbf{x}) \| p_{\theta_d}(\mathbf{z}_d|d)). & \end{aligned}$$

where the KL divergence terms are weighted by a factor β [23, 24].

Figure 3 illustrates the effects of the different terms in the above training objective. The first term of Eq. 1 involves the *likelihood* $p_{\theta_{yd}}(\mathbf{x}|\mathbf{z}_d, \mathbf{z}_y)$. It measures DIVAD’s ability to *reconstruct* an input from its latent factors, \mathbf{z}_d and \mathbf{z}_y , as shown in Figure 3a. The second and third terms act as domain-invariant and domain-specific *regularizers*, pushing the *variational posteriors* $q_{\phi_y}(\mathbf{z}_y|\mathbf{x})$ and $q_{\phi_d}(\mathbf{z}_d|\mathbf{x})$ toward their *priors* $p(\mathbf{z}_y)$ and $p_{\theta_d}(\mathbf{z}_d|d)$, respectively, as illustrated by Figure 3b. The prior $p(\mathbf{z}_y)$ will be used for anomaly scoring and further detailed in Section 5.3. The remaining distributions are

learned using neural networks:

$$\begin{aligned} p_{\theta_{yd}}(\mathbf{x}|\mathbf{z}_d, \mathbf{z}_y) &= \mathcal{N}(\text{NN}_{\theta_{yd}}(\mathbf{z}_d, \mathbf{z}_y), \text{NN}_{\sigma_{yd}}(\mathbf{z}_d, \mathbf{z}_y)) \\ p_{\theta_d}(\mathbf{z}_d|d) &= \mathcal{N}(\text{NN}_{\theta_d}(d), \text{NN}_{\sigma_d}(d)) \\ q_{\phi_y}(\mathbf{z}_y|\mathbf{x}) &= \mathcal{N}(\text{NN}_{\phi_y}(\mathbf{x}), \text{NN}_{\sigma_y}(\mathbf{x})) \\ q_{\phi_d}(\mathbf{z}_d|\mathbf{x}) &= \mathcal{N}(\text{NN}_{\phi_d}(\mathbf{x}), \text{NN}_{\sigma_d}(\mathbf{x})), \end{aligned}$$

where \mathcal{N} denotes a Gaussian distribution with mean and variance each modeled by $\text{NN}_\theta(\cdot)$, a neural network with parameters θ .

The conditional prior $p_{\theta_d}(\mathbf{z}_d|d)$ has the effect of making \mathbf{z}_d more dependent on d , by ensuring that signals from d are incorporated into \mathbf{z}_d (and thus facilitating the classification of d given \mathbf{z}_d). To further facilitate this domain classification, we add to maximum likelihood the following **domain classification** objective:

$$\mathcal{L}_d(\mathbf{x}, d; \phi_d, \omega_d) = \mathbb{E}_{q_{\phi_d}(\mathbf{z}_d|\mathbf{x})} \log q_{\omega_d}(d|\mathbf{z}_d),$$

with $\omega_d \in \Omega$ the *domain classifier parameters*. This objective amounts to training a domain classification head, by minimizing the cross-entropy loss based on the source domain labels.

We perform gradient ascent on the final maximization objective:

$$\begin{aligned} \mathcal{L}(\mathbf{x}, d; \theta_{yd}, \theta_d, \phi_d, \phi_y, \omega_d) = & \\ \mathcal{L}_{\text{ELBO}}(\mathbf{x}, d; \theta_{yd}, \theta_d, \phi_d, \phi_y) + \alpha_d \mathcal{L}_d(\mathbf{x}, d; \phi_d, \omega_d), & \end{aligned}$$

where $\alpha_d \in \mathbb{R}$ is a tradeoff hyperparameter balancing maximum likelihood estimation and domain classification. We do not share the parameters of our encoder networks NN_{ϕ_y} and NN_{ϕ_d} , but instead consider a multi-encoder architecture.

DIVAD is similar in spirit to *Domain-Invariant Variational Autoencoders* (DIVA) [24], proposed for image classification. However, our new problem setting of unsupervised anomaly detection leads to major differences from classification-based DIVA. First, by not relying on training class labels, DIVAD fuses DIVA’s class-conditioned and residual latent factors \mathbf{z}_y and \mathbf{z}_x into a single, unconditioned domain-invariant factor \mathbf{z}_y , considering a conditioning and auxiliary classification objective only for the domain-specific factor \mathbf{z}_d . Second, rather than relying on an explicit classifier on top of the class-specific factor \mathbf{z}_y , DIVAD derives its anomaly scores from these factors’ training distribution, modeled with the flexibility described in the following section.

5.3 Model Inference

Based on Definition 4, our inference goals are to: (1) find a mapping $f_y(\mathbf{x}) = \mathbf{z}_y$ from the input to domain-invariant space, and (2) model the training distribution of \mathbf{z}_y to derive our anomaly scores.

For task (1), a known result from VAE [26, 39] is that after training based on Eq. 1, the variational posterior $q_{\phi_y}(\mathbf{z}_y|\mathbf{x})$ should approximate the true posterior $p_\theta(\mathbf{z}_y|\mathbf{x})$ (dashed arrow in Figure 2b). We can therefore use it to construct our mapping f_y :

$$\mathbf{z}_y = f_y(\mathbf{x}) \sim q_{\phi_y}(\mathbf{z}_y|\mathbf{x}) \approx p_\theta(\mathbf{z}_y|\mathbf{x}).$$

For task (2), we propose two alternatives below to model the training distribution of \mathbf{z}_y : prior and aggregated posterior estimate.

5.3.1 Scoring from Prior. In the first alternative, we derive the **anomaly score** $g_W(\mathbf{x})$ of a sample \mathbf{x} as the negative log-likelihood of $f_y(\mathbf{x})$ with respect to the prior $p(\mathbf{z}_y)$:

$$g_W(\mathbf{x}) := -\log p(\mathbf{z}_y = f_y(\mathbf{x})) \quad (2)$$

The rationale behind this method is the following: First, we observe that maximizing Eq. 1 on average on the training set amounts to maximizing the regularization term of the ELBO w.r.t. \mathbf{z}_y :

$$\Omega_{\phi_y} := -\mathbb{E}_{p_{\text{train}}(\mathbf{x})} D_{\text{KL}}(q_{\phi_y}(\mathbf{z}_y|\mathbf{x})||p(\mathbf{z}_y)).$$

However, based on [49], we have the result:

$$\begin{aligned} \Omega_{\phi_y} &= \int \frac{1}{N_{\text{train}}} \sum_{i=1}^{N_{\text{train}}} q_{\phi_y}(\mathbf{z}_y|\mathbf{x}_i) \log p(\mathbf{z}_y) d\mathbf{z}_y \\ &\quad - \int \frac{1}{N_{\text{train}}} \sum_{i=1}^{N_{\text{train}}} q_{\phi_y}(\mathbf{z}_y|\mathbf{x}_i) \log q_{\phi_y}(\mathbf{z}_y|\mathbf{x}_i) d\mathbf{z}_y, \end{aligned}$$

where N_{train} is the number of training samples. By considering:

$$q_{\phi_y}(\mathbf{z}_y) = \frac{1}{N_{\text{train}}} \sum_{i=1}^{N_{\text{train}}} q_{\phi_y}(\mathbf{z}_y|\mathbf{x}_i),$$

the **marginal**, or **aggregated posterior** [5, 33] (here the empirical distribution of encoded, presumably domain-invariant, samples), we therefore have:

$$\begin{aligned} \Omega_{\phi_y} &= \int q_{\phi_y}(\mathbf{z}_y) \log p(\mathbf{z}_y) d\mathbf{z}_y \\ &\quad - \int \frac{1}{N_{\text{train}}} \sum_{i=1}^{N_{\text{train}}} q_{\phi_y}(\mathbf{z}_y|\mathbf{x}_i) \log q_{\phi_y}(\mathbf{z}_y|\mathbf{x}_i) d\mathbf{z}_y \\ \Omega_{\phi_y} &= -H(q_{\phi_y}(\mathbf{z}_y), p(\mathbf{z}_y)) + H(q_{\phi_y}(\mathbf{z}_y|\mathbf{x})), \end{aligned}$$

where $H(q_{\phi_y}(\mathbf{z}_y), p(\mathbf{z}_y))$ is the cross-entropy between the aggregated posterior and the prior, and $H(q_{\phi_y}(\mathbf{z}_y|\mathbf{x}))$ is the conditional entropy of $q_{\phi_y}(\mathbf{z}_y|\mathbf{x})$ with the empirical distribution $\hat{p}_{\text{train}}(\mathbf{x})$ [49]. As we can see, **the maximization process of the ELBO has the effect of trying to make the aggregated posterior $q_{\phi_y}(\mathbf{z}_y)$ match the prior $p(\mathbf{z}_y)$** , which *a priori* motivates the choice above of using the prior to derive anomaly scores.

Fixed Standard Gaussian Prior. We first consider the default choice of prior for \mathbf{z}_y in VAEs, as a fixed standard Gaussian:

$$p(\mathbf{z}_y) = \mathcal{N}(\mathbf{0}, \mathbf{I}),$$

and refer to the method that uses this \mathbf{z}_y prior and scores with Eq. 2 as **DIVAD-G**. A limitation of DIVAD-G is that, although the aggregated posterior and prior *should* be brought closer when maximizing the ELBO, they usually do not end up matching in practice at the end of training [5, 40]. This phenomenon is sometimes described as “*holes in the aggregated posterior*”, referring to the regions of the latent space that have high density under the prior but very low density under the aggregated posterior [8].

Learned Gaussian Mixture Prior. A method that has been shown to (at least partly) address the problem of aggregated posterior holes is to replace the fixed \mathbf{z}_y prior with a *learnable prior* $p_{\lambda}(\mathbf{z}_y)$ [8, 49], and hence have the maximization process update both the aggregated posterior and the prior. If sufficiently expressive, the prior can serve as a good approximation $\hat{q}_{\phi_y}(\mathbf{z}_y)$ of the aggregated posterior at the end of training, which makes it safer to use for anomaly scoring:

$$g_W(\mathbf{x}) := -\log p_{\lambda}(\mathbf{z}_y = f_y(\mathbf{x})) \quad (3)$$

In a way, considering a learnable prior amounts to explicitly performing a joint density estimation of the marginal likelihood

and aggregated posterior. With sufficiently expressive priors, this joint estimation also has the effect of *putting less constraints on the aggregated posterior*, letting it capture normal clusters with more variance and arbitrary shapes. This is particularly useful in AD, where the “normal” class can refer to a variety of different behaviors (even for the same entity). In practice, any density estimator $p_{\lambda}(\mathbf{z}_y)$ can be used to model the aggregated posterior. In this work, we consider a Gaussian Mixture (GM) distribution with K components:

$$p_{\lambda}(\mathbf{z}_y) = \sum_{k=1}^K w_k \mathcal{N}(\mu_k, \sigma_k^2),$$

with $\lambda = \{w_k, \mu_k, \sigma_k^2\}_{k=1}^K$ randomly initialized and trained along with the other parameters. We refer to the method that uses this \mathbf{z}_y prior and scores with Eq. 3 as **DIVAD-GM**.

5.3.2 Scoring from Aggregated Posterior Estimate. An alternative (or complementary) solution to the problem of aggregated posterior holes is to perform the density estimation of the aggregated posterior $\hat{q}_{\phi_y}(\mathbf{z}_y)$ separately, and then define the anomaly score with respect to this estimate instead of the prior:

$$g_W(\mathbf{x}) := -\log \hat{q}_{\phi_y}(\mathbf{z}_y = f_y(\mathbf{x})) \quad (4)$$

In the following, we consider this alternative in addition to the prior-based scoring for both DIVAD-G and DIVAD-GM. For DIVAD-G, the aggregated posterior is estimated by fitting a multivariate Gaussian distribution to the training samples in latent space. For DIVAD-GM, it is estimated by fitting to them a Gaussian Mixture model with the same number of components K as the prior.

5.4 Putting It All Together

We illustrate the multi-encoder architecture of our DIVAD method in Figure 4, shown here for the learned Gaussian Mixture prior detailed in Section 5.3. From this figure, we can see that encoder networks NN_{ϕ_d} and NN_{ϕ_y} take the same sample \mathbf{x} as input to output the mean and variance parameters of multivariate Gaussians $q_{\phi_d}(\mathbf{z}_d|\mathbf{x})$ and $q_{\phi_y}(\mathbf{z}_y|\mathbf{x})$, respectively. These parameters are first used to compute the KL divergence terms of Equation 1, with the parameters of the conditional prior $p_{\theta_d}(\mathbf{z}_d|\mathbf{d})$ outputted by a network NN_{θ_d} from the domain d of \mathbf{x} , and the parameters of $p_{\lambda}(\mathbf{z}_y)$ learned as described in Section 5.3. They are then used to sample the corresponding domain and class encodings of \mathbf{x} : \mathbf{z}_d and \mathbf{z}_y . These encodings, considered here of same dimension M' , are further concatenated to form the input of the decoder $\text{NN}_{\theta_{y_d}}$, outputting the parameters of the multivariate Gaussian $p_{\theta_{y_d}}(\mathbf{x}|\mathbf{z}_d, \mathbf{z}_y)$, from which the likelihood (or *reconstruction*) term of Equation 1 is computed. The bottom right of the figure finally shows the domain classification head, NN_{ω_d} , which takes the domain encoding \mathbf{z}_d of \mathbf{x} as input, and outputs the parameters of the Categorical $q_{\omega_d}(\mathbf{d}|\mathbf{z}_d)$, used to compute the domain classification objective \mathcal{L}_d .

Regarding computational cost, assuming that the encoding dimension M' and number of source domains N_{dom} are negligible compared to the input dimension $L \cdot M$ (i.e., the network is dominated by its encoder-decoder architecture), DIVAD has the same asymptotic training time as a regular VAE. In practice, DIVAD requires more training resources than VAE, as it uses (i) 2 encoder networks, resulting in twice the encodings and encoder gradients

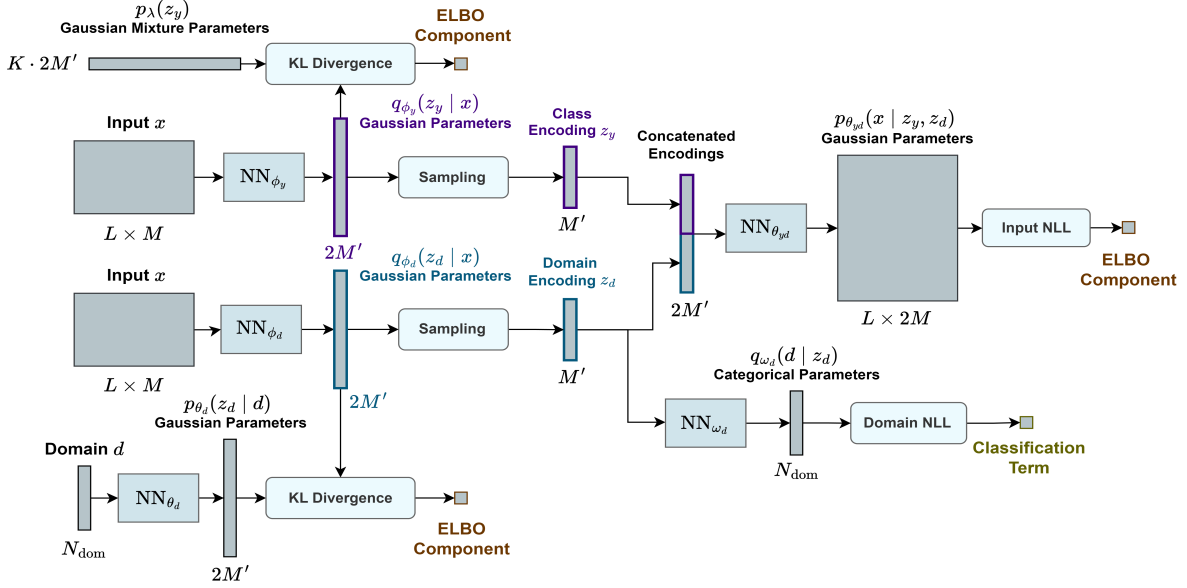


Figure 4: Multi-encoder architecture of our DIVAD-GM models, with N_{dom} the number of source domains (DIVAD-G models use a similar architecture, with the learned Gaussian Mixture parameters replaced with fixed Gaussian parameters).

to compute, and (ii) 2 encodings as input to the decoder, leading to more parameters for the first decoder layer. During inference, DIVAD incurs about half the cost of a VAE, since its anomaly scoring involves only a forward pass through a single encoder, compared to a complete input reconstruction for the VAE. Finally, using DIVAD-GM over DIVAD-G incurs modest increase in both training and inference costs, with (limited) $K \cdot 2M'$ prior parameters to learn ($2M'$ for each GM component), and K components, instead of 1, to consider when evaluating likelihoods with respect to the prior.

6 EXPERIMENTS

In this section, we evaluate the anomaly detection performance of DIVAD against existing AD methods using both the Exathlon benchmark [25] and Application Server Dataset (ASD) [30].

6.1 Experimental Setup

Our experimental setup involves different steps of the Exathlon pipeline [25]. In data preprocessing, we excluded applications 7 and 8, for which there are no disturbed and normal traces, respectively. In feature engineering, we dropped the features constant throughout the whole dataset and took the average of Spark executor features to reduce dimensionality. These steps result in $M = 237$ features to use by the AD methods.

Data Partitioning. To build a single AD model for all Spark applications, we ensure that the 8 Spark applications are represented in both the training and test sets. The training set includes normal traces and some disturbed traces to increase the variety in application *settings* and *input rates*. After data partitioning, our test sequences contain 15 Bursty Input (**T1**) anomalies; 5 Bursty Input Until Crash (**T2**) anomalies; 6 Stalled Input (**T3**) anomalies; 7 CPU Contention (**T4**) anomalies; 5 Driver Failure (**T5**) anomalies; 5 Executor Failure (**T6**) anomalies.

Training and Inference. All deep learning methods use the same random 20% of training data as validation. By default, they are

trained for 300 epochs, using a Stochastic Gradient Descent (SGD) strategy, mini-batches of size B , the AdamW optimizer [32], a weight decay coefficient of 0.01, early stopping and checkpointing on the validation loss with a patience of 100 epochs.

The hyperparameters are treated by following recommended practices [2, 6]. For *architecture parameters*, we start with the default architecture setting of each AD method as suggested in its original paper, and vary the number of hidden units, number of layers or latent dimension by a factor of 2-4, resulting in n_1 architectures per method (we generate more model variants for shallow methods, leading to larger values of n_1). Then, the *learning rate* is tuned for each architecture, considering $\eta \in \{1e-5, 3e-5, 1e-4, 3e-4\}$, and selecting the value that yields the lowest validation loss (i.e., the best *modeling performance* [6]). The *batch size* is method-dependent and set to the value used in the method’s original paper (or if absent, to 32 by default). This entails n_1 trained models per method, each with its “best” learning rate and recommended batch size. At inference time (running each model on the test sequences), we derive the record scoring function g using a grid of 12 *anomaly score smoothing factors* γ , leading to $12n_1$ runs per AD method. We further filter out the architectures whose runs give overall poor performance, resulting in $12n_2$ runs, with $n_2 \leq n_1$, per AD method.

We evaluate AD methods based on their *point-based* AD performance, using the **peak F1-score** metric of the Exathlon benchmark (i.e., the “best”-possible F1-score on the Precision-Recall curve). When computing F1-scores, we average Recall values across different event types. We finally summarize the performance of each AD method, in terms of peak F1-score, using a box-plot over its $12n_2$ model runs. Additional details are available in Appendix A.6.

Representative AD Methods. Our analysis compares DIVAD to 13 unsupervised AD methods, either performing a *point modeling* (i.e., window length $L = 1$) or *sequence modeling* (window length $L > 1$) of the data. The unsupervised AD methods are further

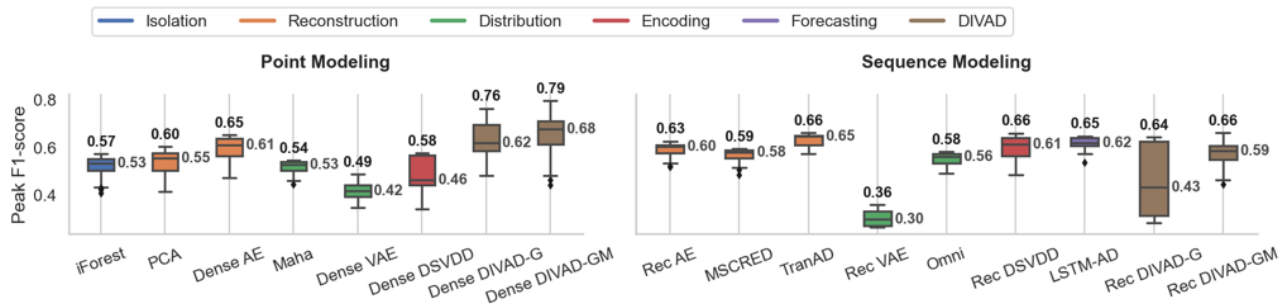


Figure 5: Box plots of peak F1-scores achieved by the existing and DIVAD methods, separated by modeling strategy (point vs. sequence) and colored by method category (from Schmidl et al. [45] plus DIVAD).

grouped based on their anomaly scoring strategy, as per the taxonomy of Schmidl et al. [45] discussed in Section 2.

We include the following **point modeling** AD methods in our study (details about these methods and hyperparameters considered are given in Appendix B.2): (1) Isolation forest [31] (**iForest**), as the most popular isolation tree method; (2-3) Principal Component Analysis (**PCA**) [47] and Dense Autoencoder (**Dense AE**) [21, 44], as representative and popular shallow and deep reconstruction methods, respectively; (4) Dense Deep SVDD [42] (**Dense DSVD**), as a recent and popular encoding method; (5-6) Mahalanobis [3, 47] (**Maha**) and Dense Variational Autoencoder (**Dense VAE**) [7], as representative shallow and deep distribution methods, respectively.

We include the following **sequence modeling** methods (with further details given in Appendix B.3): (7-9) Recurrent Autoencoder [21, 44] (**Rec AE**), **MSCRED** [57] and **TranAD** [50], as the sequence modeling version of Dense AE and more recent reconstruction methods, respectively; (10) **LSTM-AD** [34], as the most popular forecasting method; (11) Recurrent Deep SVDD [42] (**Rec DSVD**) as the sequence modeling version of the Dense DSVD encoding method; (12-13) Recurrent VAE (**Rec VAE**) and OmniAnomaly [48] (**Omni**) as the sequence modeling version of Dense VAE and a more recent distribution method, respectively. We also tried to include the more recent encoding method DCDetector [56], but did not retain it due to its poor performance on our dataset.

DIVAD Variants. This study considers 4 DIVAD variants, either performing a point modeling or sequence modeling of the data. The point modeling variants, referred to as **Dense DIVAD-G** and **Dense DIVAD-GM**, use a fully-connected architecture for the encoders NN_{ϕ_d} , NN_{ϕ_y} and decoder $NN_{\theta_{y_d}}$. The sequence modeling variants, referred to as **Rec DIVAD-G** and **Rec DIVAD-GM**, use recurrent architectures instead (more details are in Appendix C). We employ the same hyperparameter selection strategy for DIVAD variants as the other DL methods, considering KL divergence weights $\beta \in \{1, 5\}$ (i.e., a regular VAE and β -VAE [23] framework with increased latent space regularization), and a domain classification weight $\alpha_d = 100,000$ set based on the scale we observed for the losses \mathcal{L}_{ELBO} and \mathcal{L}_d in initial experiments. We study the sensitivity of DIVAD to those two hyperparameters in Section 6.2.6.

6.2 Results and Analyses using Exathlon

For the Exathlon benchmark (detailed in §3), Figure 5 shows the box plots of the peak F1-scores achieved by the DIVAD variants and

13 AD methods across their hyperparameter values. It separates point from sequence modeling methods into two subplots with a shared y-axis, with boxes colored based on the method category.

6.2.1 Existing AD Methods. Our main observations about existing AD methods are the following: (1) The best performance achieved is the maximum peak F1-score of 0.66 by TranAD, which is not highly accurate. (2) Across different categories, *reconstruction methods performed the best* (with a maximum peak F1-score of 0.66 by TranAD) *while distribution methods performed the worst* on average (with a maximum peak F1-score of 0.58 by OmniAnomaly). These results are also consistent with the study of [50], which reported that TranAD outperformed OmniAnomaly and MSCRED. (3) The use of deep learning was beneficial among reconstruction methods, while it tended to degrade performance for distribution methods—our subsequent domain shift analysis will explain this behavior.

6.2.2 Analysis of Domain Shift. Figure 6 illustrates the impact of domain shift on AD methods by showing the Kernel Density Estimate (KDE) plots of the anomaly scores they assigned to the training normal, test normal, and test anomalous records. On these plots, the separation between the anomaly scores assigned to the test normal and test anomalous records (i.e., between the **blue** and **red** KDEs) directly relates to the AD performance of a method. As illustrated for the point modeling reconstruction and distribution methods, all the methods have the test normal scores and test anomalous scores overlapping, hence the limited detection accuracy.

Furthermore, the overlap between the scores of training normal and test normal records (i.e., **green** and **blue** KDEs) reflects its “robustness” to the domain shift from training to test data. (1) Comparing Figures 6c to 6a and 6d to 6b, respectively, we can see that distribution methods, by modeling the training distribution more *explicitly*, tended to produce more similar anomaly scores across the training normal records (i.e., tighter **green** KDEs). However, this tighter modeling of the training distribution also made these methods more sensitive to domain shift, deeming test normal and test anomalous records “similarly anomalous” (i.e., high **blue** and **red** KDEs overlap), which hindered their performance. (2) Comparing Figures 6b to 6a and 6d to 6c, we see that deep methods achieved a better separation between the training normal and test anomalous records, by modeling the training data at a finer level than shallow methods. At the same time, they suffer from a larger separation between the training normal and test normal records, indicating their sensitivity to domain shifts. In both cases, **the more a method**

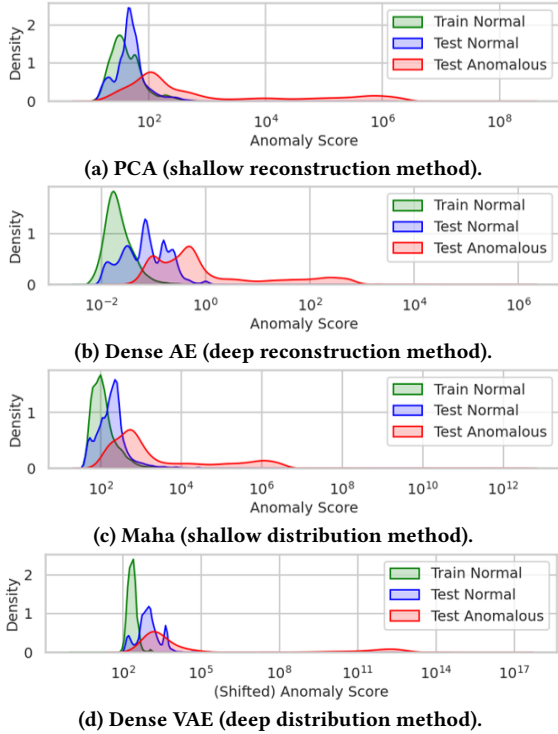


Figure 6: Kernel Density Estimate (KDE) plots of the anomaly scores assigned by reconstruction and distribution methods to training normal, test normal and test anomalous records.

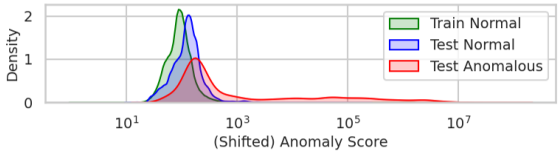


Figure 7: KDE plots of the anomaly scores assigned by Omni to training normal, test normal, and test anomalous records.

precisely and explicitly models the training data, the more vulnerable it is to the domain shift challenge. Figure 7 shows a similar plot for OmniAnomaly. We can see that its anomaly scores assigned to training normal records and test anomalies overlapped significantly, indicating a shortcoming in normal data modeling, despite this method being distribution-based and converging properly. Since Omni corresponds to a more advanced extension of VAE (with a non-Gaussian temporal modeling of latent variables), nontrivial extensions could be required to exploit its modeling potential and (at least) match the behavior of Dense VAE.

6.2.3 DIVAD vs. Existing AD Methods. We now examine DIVAD’s performance. First, Figure 5 shows that **Dense DIVAD-GM and Dense DIVAD-G significantly outperform the SOTA method TranAD in maximum performance**, achieving 20% and 15% improvements in maximum peak F1-scores (0.79 and 0.76 over 0.66), respectively. Between the variants, using a learned Gaussian Mixture prior (DIVAD-GM) instead of a fixed Gaussian prior (DIVAD-G) is beneficial in improving both the maximum and median peak F1-scores for the point and sequence modeling variants.

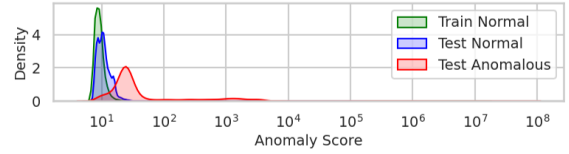


Figure 8: KDE plots of the anomaly scores assigned by Dense DIVAD-GM to training normal, test normal, and test anomalous records.

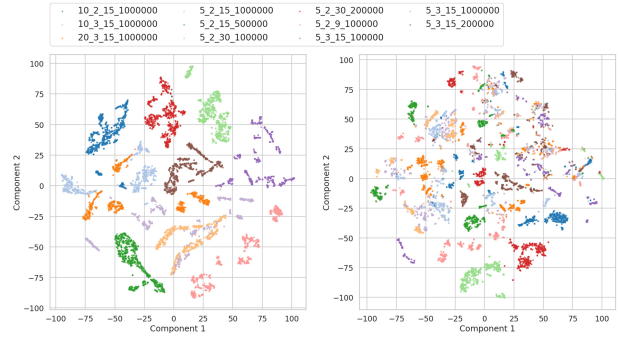


Figure 9: t-SNE scatter plots of Dense DIVAD-GM’s domain-specific (left) and domain-invariant (right) encodings of test normal records, undersampled to 10,000 records, balanced and colored by domain.

Second, **the higher performance of Dense DIVAD-GM can be directly attributed to its accurate domain generalization.** To illustrate this, Figure 9 shows t-SNE scatter plots of the domain-specific and domain-invariant encodings it produced for test normal records (sampled from $q_{\phi_d}(z_d|\mathbf{x})$ and $q_{\phi_y}(z_y|\mathbf{x})$, respectively), undersampled to 10,000 data records, balanced and colored by domain. We can see that the mapping learned by Dense DIVAD-GM from the *input* to its *domain-specific* space produced the distinct domain clusters expected, while the mapping learned from the *input* to its *domain-invariant* space produced more scattered encodings.

Furthermore, Figure 8 shows the KDE plots of the anomaly scores assigned by the best-performing Dense DIVAD-GM to the training normal, test normal and test anomalous records. We see that the explicit modeling of the training data distribution by Dense DIVAD-GM led to a similar benefit as Dense VAE (see Figure 6d), with a low variance in the anomaly scores assigned to the training normal records. Contrary to Dense VAE, Dense DIVAD-GM performed this precise density estimation in a *domain-invariant* space (where distribution shifts were drastically reduced), which made it generalize to *test* normal records as well (i.e., better *aligned* and similarly narrow **green** and **blue** KDEs). As such, Dense DIVAD-GM could generally view test anomalies as “more abnormal” than test normal records, which led to the better performance.

6.2.4 DIVAD Variants. Another observation we can make from Figure 5 is that *point modeling DIVAD variants could outperform TranAD for our dataset and experimental setup, while sequence modeling variants could not.* Point modeling variants being sufficient here can be explained by the dataset’s event types being *mostly reflected as contextual anomalies* given our features (i.e., data records that are anomalous in a given context/*domain*, but normal in some others). Figure 10 illustrates this by showing KDE plots of the *last completed batch processing delay* feature over normal data and T1 (Bursty Input) events. The top plot shows the distributions for a

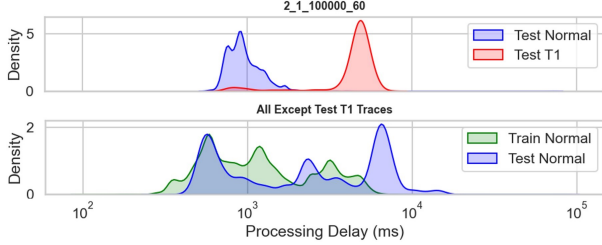


Figure 10: KDE plots of the last completed batch processing delay for training normal data, test normal data, and test anomalous data in a Bursty Input (T1) trace (top) and non-T1 traces (bottom).

given test T1 trace, while the bottom plot shows them for the remaining data, using the same x-axis in log scale. We can see that, although T1 events induce higher processing delays than normal *within the context of a trace*, these “higher” values actually appear normal with respect to the training and test normal data globally, in particular, in some other *contexts/domains*. When viewed in the domain-invariant spaces of our DIVAD methods, such contextual anomalies could typically be turned into *point* anomalies (data records deviating from the rest of the data, no matter the context). Referring back to the central assumption of DIVAD, considering *feature combinations* at *single time steps* at a time was here sufficient for the point modeling methods to learn domain-invariant patterns, given that most anomalies in Exathlon are of the contextual type.

The lower performance observed for sequence modeling DIVAD variants could be explained by the *heightened challenge of learning domain-invariant patterns in the sequential setting*. While leveraging sequential information can be useful in theory, identifying domain-invariant *shapes* within and across $M = 237$ time series constitutes a harder task than relying on simple feature combinations at given time steps for our dataset and setup. This can be verified using the anomaly score distributions, with a higher overlap between the test normal and abnormal records explaining the lower performance.

6.2.5 Sensitivity to Anomaly Scoring Strategy. Figure 11 presents a sensitivity analysis of the anomaly scoring strategy used by our DIVAD methods. It shows the box plots of peak F1-scores achieved by each DIVAD variant and anomaly scoring strategy, with “(P)” indicating the scoring is based on the class encoding *prior* (fixed Gaussian for DIVAD-G, learned Gaussian Mixture for DIVAD-GM), and “(AP)” indicating the scoring is based on the class encoding *aggregated posterior* (estimated as a Gaussian for DIVAD-G, and as a Gaussian Mixture with K components for DIVAD-GM). As we can see from this figure, sequence modeling DIVAD methods again performed worse than the point modeling variants in both median and maximum peak F1-scores no matter the scoring strategy used. Like expected, **deriving the anomaly scores from an aggregated posterior estimate instead of the prior was significantly beneficial for both DIVAD-G methods**, which, by relying on a fixed Gaussian prior, are particularly subject to the issue of “holes in the aggregated posterior” discussed in Section 5.3. By relying on a *more expressive* and *learned* class encoding prior, **DIVAD-GM was less sensitive to the type of scoring strategy used**, with the scoring based on the prior performing better in point modeling, and the one based on the aggregated posterior performing better in sequence modeling. This observation is consistent with our expectations, and

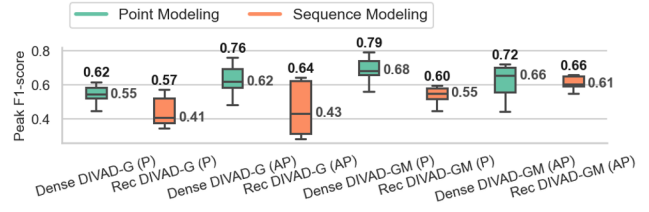


Figure 11: Box plots of peak F1-scores achieved by each DIVAD variant and anomaly scoring strategy (class encoding prior (P) vs. aggregated posterior (AP)), colored by modeling strategy.

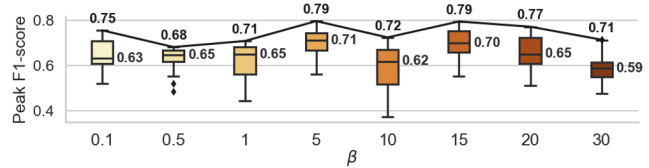


Figure 12: Box plots of peak F1-scores achieved by Dense DIVAD-GM for different KL divergence weights β .

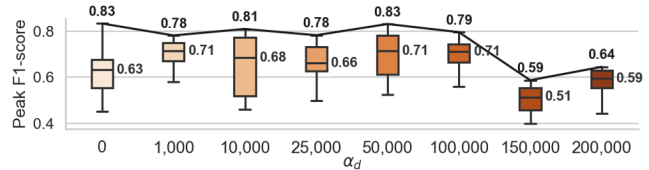


Figure 13: Box plots of peak F1-scores achieved by Dense DIVAD-GM for different domain classification weights α_d .

motivated our choice of including both scoring strategies into the hyperparameters grid of DIVAD-GM in our study.

6.2.6 Sensitivity to Hyperparameters. Figure 12 shows the box plots of peak F1-scores achieved by Dense DIVAD-GM across different KL divergence weights β . From this figure, we can see that finding an optimal β value improves both the maximum and median performance significantly (by up to 16% and 20%, respectively, from the worst value). The benefit of Dense DIVAD-GM over other AD methods, however, remains robust across all β values tested (recall that the best peak F1-score of other AD methods is 0.66).

Figure 13 shows the peak F1-scores achieved by Dense DIVAD-GM across different domain classification weights α_d . We see that its maximum peak F1-score is robust across low and medium α_d values, with some even yielding better results than the value of 100,000 selected for our study. This figure also shows that obtaining the best performance is possible even without domain classification head NN_{ω_d} (i.e., setting $\alpha_d = 0$). However, enforcing domain information via NN_{ω_d} helps reduce Dense DIVAD-GM’s sensitivity to other hyperparameters, enabling it to outperform existing methods more *consistently*, with significantly higher median and upper quartile peak F1-scores for suitable α_d values than for $\alpha_d = 0$.

6.2.7 Training and Inference Times. Table 1 shows the average time of training and inference steps (one step per mini-batch of size $B = 32$) for the VAE and DIVAD variants on an NVIDIA A100 80GB PCIe, with hyperparameters adjusted to make DIVAD and VAE directly comparable (details are in Appendix E). This table shows the expected trend for training: DIVAD’s training steps take about

Table 1: Training and inference times for DIVAD and VAE.

Method	Training Step (ms)	Inference Step (ms)
Dense VAE [7]	3.3	19.4
Dense DIVAD-G	7.3	9.1
Dense DIVAD-GM	9.7	8.9
Rec VAE [7]	7.2	28.1
Rec DIVAD-G	11.6	12.9
Rec DIVAD-GM	13.3	12.4

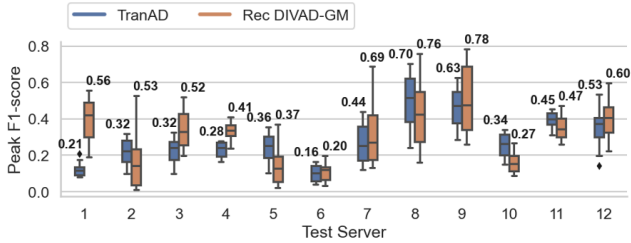


Figure 14: Box plots of peak F1-scores achieved by TranAD and Rec DIVAD-GM for ASD, using each server as a test set.

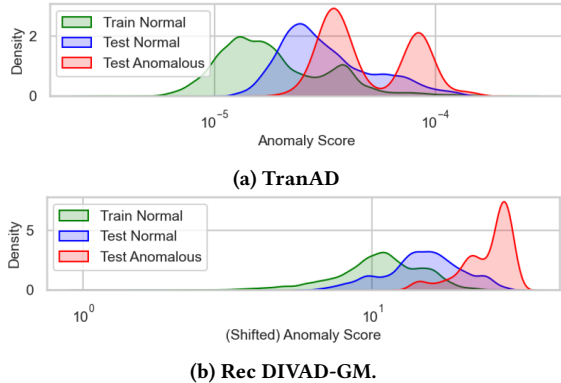


Figure 15: KDE plots of the anomaly scores assigned by TranAD and Rec DIVAD-GM to ASD’s data records, using server 1 as test.

twice the time of VAE’s, and DIVAD-GM takes 16.5% longer than DIVAD-G on average for a given architecture. During inference, Table 1 confirms that DIVAD takes less than half the time of VAE, with no significant difference between DIVAD-G and DIVAD-GM.

6.3 Broader Applicability: ASD Use Case

We now study the broader applicability of our DIVAD framework using the Application Server Dataset (ASD) [30]. This dataset, collected from a large Internet company, consists of 12 *traces*, each of which recorded the status of a group of services running on a separate *server*, using 19 metrics every five minutes. The goal is to detect the labeled anomaly ranges located at the end of the traces. The anomaly ratio is 4.61%, with minimum, median and maximum anomaly lengths of 3, 18 and 235 data records, respectively.

In this study, we use ASD to assess the extent to which our DIVAD framework can learn *server-invariant* normal patterns to detect anomalies in a new, *unseen* test server. As such, our experimental setup considers 11 out of the 12 traces as training (without the anomalies) for a single model instance, and the remaining trace as test. For these 12 runs, we report the performance of TranAD (the

best-performing existing method) and Rec DIVAD-GM. This time, Rec DIVAD-GM indeed outperformed Dense DIVAD-GM in our experiments, most likely due to (i) a higher presence of *collective* anomalies in ASD (i.e., data records that are anomalous collectively, but not individually), and (ii) the lower number of features $M = 19$, making it easier to identify meaningful domain-invariant shapes among them. We consider a window length $L = 20$ for both methods, and the same model training and selection strategy as in the previous study. More details can be found in Appendix F.

Figure 14 presents the results of our 12 tests, showing the box plots of peak F1-scores achieved by TranAD and Rec DIVAD-GM across their hyperparameter values for each test server. We see that Rec DIVAD-GM outperforms TranAD in maximum peak F1-score for 11 out of 12 test servers (i.e., 92% of the cases), improving the maximum performance by more than 10% for 8 of them. These results also show that the *median* performance is improved by Rec DIVAD-GM for 7 out of the 12 test servers, indicating the sensitivity of DIVAD with respect to hyperparameters, and the necessity of properly tuning them to benefit from a performance gain.

Figures 15a and 15b show the KDE plots of the anomaly scores assigned by the best-performing TranAD and Rec DIVAD-GM to training normal, test normal, and test anomalous records when using server 1 as a test set (i.e., the setup for which Rec DIVAD-GM improved the performance the most, by 167%). From Figure 15a, we can see that the low performance of TranAD was primarily to the lower mode of its distribution of anomaly scores assigned to anomalies, which had a significant overlap, and thus were considered “similarly abnormal”, to some test normal data. As shown in Figure 15b, Rec DIVAD-GM was able to alleviate this issue, producing much less overlap between this lower mode and the rest of test normal data, which explains the performance gain.

7 CONCLUSIONS AND FUTURE DIRECTIONS

This paper presented a unified framework for benchmarking anomaly detection (AD) methods, and highlighted the problem of *shifts* in normal behavior in practical AIops scenarios. We then formally formulated the AD problem under domain shift and proposed a new approach, Domain-Invariant VAE for Anomaly Detection (DIVAD), to learn domain-invariant representations for effective anomaly detection in unseen domains. Evaluation results show that the two main DIVAD variants significantly outperform the best unsupervised AD method using the Exathlon benchmark, with 15-20% improvements in maximum peak F1-scores, and can be applied to the Application Server Dataset to demonstrate broader applicability.

Our future research directions include a *weakly-supervised* extension of DIVAD, combining its explicit modeling of normal behavior shifts with a higher robustness to removing anomaly signals enabled by a few training anomalies, and enhancing the model with *explainability*, indicating the reasons behind anomalies, which will be key to widespread adoption in real-world use cases.

REFERENCES

- [1] Martín Abadi, Paul Barham, Jianmin Chen, Zhifeng Chen, Andy Davis, Jeffrey Dean, Matthieu Devin, Sanjay Ghemawat, Geoffrey Irving, Michael Isard, Manjunath Kudlur, Josh Levenberg, Rajat Monga, Sherry Moore, Derek G. Murray, Benoit Steiner, Paul Tucker, Vijay Vasudevan, Pete Warden, Martin Wicke, Yuan Yu, and Xiaoqiang Zheng. 2016. TensorFlow: a system for large-scale machine learning. In *Proceedings of the 12th USENIX Conference on Operating Systems*

- Design and Implementation* (Savannah, GA, USA) (OSDI'16). USENIX Association, USA, 265–283.
- [2] Charu C. Aggarwal. 2017. *An Introduction to Outlier Analysis*. Springer International Publishing, Cham, 1–34. https://doi.org/10.1007/978-3-319-47578-3_1
 - [3] Charu C. Aggarwal. 2017. *Linear Models for Outlier Detection*. Springer International Publishing, Cham, 65–110. https://doi.org/10.1007/978-3-319-47578-3_3
 - [4] Kei Akuzawa, Yusuke Iwasawa, and Yutaka Matsuo. 2020. Adversarial Invariant Feature Learning with Accuracy Constraint for Domain Generalization. In *Machine Learning and Knowledge Discovery in Databases*, Ulf Brefeld, Elisa Fromont, Andreas Hotho, Arno Knobbe, Marloes Maathuis, and Céline Robardet (Eds.). Springer International Publishing, Cham, 315–331.
 - [5] Alexander A. Alemi, Ben Poole, Ian Fischer, Joshua V. Dillon, Rif A. Saurous, and Kevin Murphy. 2018. Fixing a Broken ELBO. arXiv:1711.00464 [cs.LG]
 - [6] Sarah Alnegheimish, Dongyu Liu, Carles Sala, Laure Berti-Equille, and Kalyan Veeramachani. 2022. Sintel: A Machine Learning Framework to Extract Insights from Signals. In *Proceedings of the 2022 International Conference on Management of Data* (Philadelphia, PA, USA) (SIGMOD '22). Association for Computing Machinery, New York, NY, USA, 1855–1865. <https://doi.org/10.1145/3514221.3517910>
 - [7] Jinwon An and Sungzoon Cho. 2015. Variational Autoencoder based Anomaly Detection using Reconstruction Probability. In *Special Lecture on IE*. <https://api.semanticscholar.org/CorpusID:36663713>
 - [8] Matthias Bauer and Andriy Mnih. 2019. Resampled Priors for Variational Autoencoders. arXiv:1810.11428 [stat.ML]
 - [9] Li Bu, Dongbin Zhao, and Cesare Alippi. 2017. An incremental change detection test based on density difference estimation. *IEEE Transactions on Systems, Man, and Cybernetics: Systems* 47, 10 (2017), 2714–2726.
 - [10] Varun Chandola, Arindam Banerjee, and Vipin Kumar. 2009. Anomaly Detection: A Survey. *ACM Comput. Surv.* 41, 3, Article 15 (jul 2009), 58 pages. <https://doi.org/10.1145/1541880.1541882>
 - [11] Zahra Zamanzadeh Darban, Geoffrey I. Webb, Shirui Pan, Charu C. Aggarwal, and Mahsa Salehi. 2022. Deep Learning for Time Series Anomaly Detection: A Survey. arXiv:2211.05244 [cs.LG]
 - [12] Joshua V. Dillon, Ian Langmore, Dustin Tran, Eugene Brevdo, Srinivas Vasudevan, Dave Moore, Brian Patton, Alex Alemi, Matt Hoffman, and Rif A. Saurous. 2017. TensorFlow Distributions. arXiv:1711.10604 [cs.LG] <https://arxiv.org/abs/1711.10604>
 - [13] Kota Dohi, Keisuke Imoto, Noboru Harada, Daisuke Niizumi, Yuma Koizumi, Tomoya Nishida, Harsh Purohit, Ryo Tanabe, Takashi Endo, Masaaki Yamamoto, and Yohei Kawaguchi. 2022. Description and Discussion on DCASE 2022 Challenge Task 2: Unsupervised Anomalous Sound Detection for Machine Condition Monitoring Applying Domain Generalization Techniques. In *Proceedings of the 7th Detection and Classification of Acoustic Scenes and Events 2022 Workshop (DCASE2022)*. Nancy, France, 1–5.
 - [14] Denis Moreira Dos Reis, Peter Flach, Stan Matwin, and Gustavo Batista. 2016. Fast unsupervised online drift detection using incremental kolmogorov-smirnov test. In *Proceedings of the 22nd ACM SIGKDD international conference on knowledge discovery and data mining*. 1545–1554.
 - [15] João Gama, Indrė Žliobaitė, Albert Bifet, Mykola Pechenizkiy, and Abdelhamid Bouchachia. 2014. A survey on concept drift adaptation. *ACM computing surveys (CSUR)* 46, 4 (2014), 1–37.
 - [16] Yaroslav Ganin, Evgeniya Ustinova, Hana Ajakan, Pascal Germain, Hugo Larochelle, François Laviolette, Mario Marchand, and Victor Lempitsky. 2016. Domain-adversarial training of neural networks. *J. Mach. Learn. Res.* 17, 1 (jan 2016), 2096–2030.
 - [17] Gartner. 2018. Market Guide for AIOps Platforms. <https://www.gartner.com/en/documents/3772124>. Accessed: 2023-10-10.
 - [18] Rick Groenendijk, Sezer Karaoglu, Theo Gevers, and Thomas Mensink. 2020. Multi-Loss Weighting with Coefficient of Variations. In *Proceedings of the IEEE/CVF Winter Conference on Applications of Computer Vision*. 1469–1478.
 - [19] Manish Gupta, Jing Gao, Charu C. Aggarwal, and Jiawei Han. 2014. Outlier Detection for Temporal Data: A Survey. *IEEE Transactions on Knowledge and Data Engineering* 26, 9 (2014), 2250–2267.
 - [20] D. M. Hawkins. 1980. *Identification of outliers*. Chapman and Hall, London [u.a.].
 - [21] Simon Hawkins, Hongxing He, Graham Williams, and Rohan Baxter. 2002. Outlier Detection Using Replicator Neural Networks. In *Data Warehousing and Knowledge Discovery*, Yahiko Kambayashi, Werner Winiwarter, and Masatoshi Arikawa (Eds.). Springer Berlin Heidelberg, Berlin, Heidelberg, 170–180.
 - [22] Huan He, Owen Queen, Teddy Koker, Consuelo Cuevas, Theodoros Tsiligkaridis, and Marinka Zitnik. 2023. Domain Adaptation for Time Series Under Feature and Label Shifts. arXiv:2302.03133 [cs.LG]
 - [23] Irina Higgins, Loic Matthey, Arka Pal, Christopher P. Burgess, Xavier Glorot, Matthew M. Botvinick, Shakir Mohamed, and Alexander Lerchner. 2016. beta-VAE: Learning Basic Visual Concepts with a Constrained Variational Framework. In *International Conference on Learning Representations*. <https://api.semanticscholar.org/CorpusID:46798026>
 - [24] Maximilian Ilse, Jakob M. Tomczak, Christos Louizos, and Max Welling. 2020. DIVA: Domain Invariant Variational Autoencoders. In *Proceedings of the Third Conference on Medical Imaging with Deep Learning (Proceedings of Machine Learning Research)*, Vol. 121. PMLR, 322–348. <https://proceedings.mlr.press/v121/ilse20a.html>
 - [25] Vincent Jacob, Fei Song, Arnaud Stiegler, Bijan Rad, Yanlei Diao, and Nesime Tatbul. 2021. Exathlon: A Benchmark for Explainable Anomaly Detection over Time Series. *Proc. VLDB Endow.* 14, 11 (jul 2021), 2613–2626. <https://doi.org/10.14778/3476249.3476307>
 - [26] Diederik P Kingma and Max Welling. 2013. Auto-Encoding Variational Bayes. arXiv:1312.6114 [stat.ML]
 - [27] Naveen Kodali, James Hays, Jacob D. Abernethy, and Zsolt Kira. 2018. On Convergence and Stability of GANs. *arXiv: Artificial Intelligence* (2018). <https://api.semanticscholar.org/CorpusID:37428828>
 - [28] Yann LeCun, Yoshua Bengio, and Geoffrey Hinton. 2015. Deep learning. *nature* 521, 7553 (2015), 436.
 - [29] Ya Li, Xinmei Tian, Mingming Gong, Yajing Liu, Tongliang Liu, Kun Zhang, and Dacheng Tao. 2018. Deep Domain Generalization via Conditional Invariant Adversarial Networks. In *Computer Vision – ECCV 2018*, Vittorio Ferrari, Martial Hebert, Cristian Sminchisescu, and Yair Weiss (Eds.). Springer International Publishing, Cham, 647–663.
 - [30] Zhihan Li, Youjian Zhao, Jiaqi Han, Ya Su, Rui Jiao, Xidao Wen, and Dan Pei. 2021. Multivariate Time Series Anomaly Detection and Interpretation Using Hierarchical Inter-Metric and Temporal Embedding. In *Proceedings of the 27th ACM SIGKDD Conference on Knowledge Discovery & Data Mining* (Virtual Event, Singapore) (KDD '21). Association for Computing Machinery, New York, NY, USA, 3220–3230. <https://doi.org/10.1145/3447548.3467075>
 - [31] Fei Tony Liu, Kai Ming Ting, and Zhi-Hua Zhou. 2008. Isolation Forest. In *2008 Eighth IEEE International Conference on Data Mining*. 413–422. <https://doi.org/10.1109/ICDM.2008.17>
 - [32] Ilya Loshchilov and Frank Hutter. 2019. Decoupled Weight Decay Regularization. In *7th International Conference on Learning Representations, ICLR 2019, New Orleans, LA, USA, May 6-9, 2019*. OpenReview.net. <https://openreview.net/forum?id=Bkg6RiCqY7>
 - [33] Alireza Makhzani, Jonathon Shlens, Navdeep Jaitly, Ian Goodfellow, and Brendan Frey. 2016. Adversarial Autoencoders. arXiv:1511.05644 [cs.LG]
 - [34] Pankaj Malhotra, Lovekesh Vig, Gautam M. Shroff, and Puneet Agarwal. 2015. Long Short Term Memory Networks for Anomaly Detection in Time Series. In *The European Symposium on Artificial Neural Networks*. <https://api.semanticscholar.org/CorpusID:43680425>
 - [35] Toshihiko Matsuura and Tatsuya Harada. 2019. Domain Generalization Using a Mixture of Multiple Latent Domains. In *AAAI Conference on Artificial Intelligence*. <https://api.semanticscholar.org/CorpusID:208138410>
 - [36] F. Pedregosa, G. Varoquaux, A. Gramfort, V. Michel, B. Thirion, O. Grisel, M. Blondel, P. Prettenhofer, R. Weiss, V. Dubourg, J. Vanderplas, A. Passos, D. Cournapeau, M. Brucher, M. Perrot, and E. Duchesnay. 2011. Scikit-learn: Machine Learning in Python. *Journal of Machine Learning Research* 12 (2011), 2825–2830.
 - [37] Vihari Piratla, Praneeth Netrapalli, and Sunita Sarawagi. 2020. Efficient Domain Generalization via Common-Specific Low-Rank Decomposition. In *Proceedings of the 37th International Conference on Machine Learning, ICML 2020, 13-18 July 2020, Virtual Event (Proceedings of Machine Learning Research)*, Vol. 119. PMLR, 7728–7738. <https://proceedings.mlr.press/v119/piratla20a.html>
 - [38] Fengchun Qiao, Long Zhao, and Xi Peng. 2020. Learning to Learn Single Domain Generalization. In *2020 IEEE/CVF Conference on Computer Vision and Pattern Recognition (CVPR)*. 12553–12562. <https://doi.org/10.1109/CVPR42600.2020.01257>
 - [39] Danilo Jimenez Rezende, Shakir Mohamed, and Daan Wierstra. 2014. Stochastic Backpropagation and Approximate Inference in Deep Generative Models. In *Proceedings of the 31st International Conference on Machine Learning (Proceedings of Machine Learning Research)*, Eric P. Xing and Tony Jebara (Eds.), Vol. 32. PMLR, Beijing, China, 1278–1286. <https://proceedings.mlr.press/v32/rezende14.html>
 - [40] Mihaela Rosca, Balaji Lakshminarayanan, and Shakir Mohamed. 2019. Distribution Matching in Variational Inference. arXiv:1802.06847 [stat.ML]
 - [41] Kevin Roth, Aurélien Lucchi, Sebastian Nowozin, and Thomas Hofmann. 2017. Stabilizing Training of Generative Adversarial Networks through Regularization. In *Neural Information Processing Systems*. <https://api.semanticscholar.org/CorpusID:23519254>
 - [42] Lukas Ruff, Robert Vandermeulen, Nico Goernitz, Lucas Deecke, Shoaib Ahmed Siddiqui, Alexander Binder, Emmanuel Müller, and Marius Kloft. 2018. Deep One-Class Classification. In *Proceedings of the 35th International Conference on Machine Learning (Proceedings of Machine Learning Research)*, Jennifer Dy and Andreas Krause (Eds.), Vol. 80. PMLR, 4393–4402. <https://proceedings.mlr.press/v80/ruff18a.html>
 - [43] Lukas Ruff, Robert A. Vandermeulen, Nico Goernitz, Alexander Binder, Emmanuel Müller, Klaus-Robert Müller, and Marius Kloft. 2020. Deep Semi-Supervised Anomaly Detection. In *International Conference on Learning Representations*. <https://openreview.net/forum?id=HkgH0TEYWH>
 - [44] Mayu Sakurada and Takehisa Yairi. 2014. Anomaly Detection Using Autoencoders with Nonlinear Dimensionality Reduction. In *Proceedings of the MLSDA 2014 2nd Workshop on Machine Learning for Sensory Data Analysis* (Gold Coast, Australia QLD, Australia) (MLSDA'14). Association for Computing Machinery,

- New York, NY, USA, 4–11. <https://doi.org/10.1145/2689746.2689747>
- [45] Sebastian Schmidl, Phillip Wenig, and Thorsten Papenbrock. 2022. Anomaly Detection in Time Series: A Comprehensive Evaluation. *Proc. VLDB Endow.* 15, 9 (may 2022), 1779–1797. <https://doi.org/10.14778/3538598.3538602>
- [46] Rui Shao, Xiangyuan Lan, Jiawei Li, and Pong C. Yuen. 2019. Multi-Adversarial Discriminative Deep Domain Generalization for Face Presentation Attack Detection. In *The IEEE Conference on Computer Vision and Pattern Recognition (CVPR)*.
- [47] Mei-Ling Shyu, Shu-Ching Chen, Kanoksri Sarinnapakorn, and Liwu Chang. 2003. A Novel Anomaly Detection Scheme Based on Principal Component Classifier. In *Proceedings of International Conference on Data Mining*.
- [48] Ya Su, Youjian Zhao, Chenhao Niu, Rong Liu, Wei Sun, and Dan Pei. 2019. Robust Anomaly Detection for Multivariate Time Series through Stochastic Recurrent Neural Network. In *Proceedings of the 25th ACM SIGKDD International Conference on Knowledge Discovery & Data Mining (Anchorage, AK, USA) (KDD '19)*. Association for Computing Machinery, New York, NY, USA, 2828–2837. <https://doi.org/10.1145/3292500.3330672>
- [49] Jakub M. Tomczak. [n.d.]. Priors in VAEs. https://jmtomczak.github.io/blog/7/7_priors.html. Accessed: 2023-12-26.
- [50] Shreshth Tuli, Giuliano Casale, and Nicholas R. Jennings. 2022. TranAD: Deep Transformer Networks for Anomaly Detection in Multivariate Time Series Data. *Proc. VLDB Endow.* 15, 6 (feb 2022), 1201–1214. <https://doi.org/10.14778/3514061.3514067>
- [51] Laurens van der Maaten and Geoffrey Hinton. 2008. Visualizing Data using t-SNE. *Journal of Machine Learning Research* 9, 86 (2008), 2579–2605. <http://jmlr.org/papers/v9/vandermaaten08a.html>
- [52] Satvik Venkatesh, Gordon Wichern, Aswin Subramanian, and Jonathan Le Roux. 2022. *Disentangled surrogate task learning for improved domain generalization in unsupervised anomalous sound detection*. Technical Report. DCASE2022 Challenge.
- [53] Jindong Wang, Cuiling Lan, Chang Liu, Yidong Ouyang, Tao Qin, Wang Lu, Yiqiang Chen, Wenjun Zeng, and Philip S. Yu. 2023. Generalizing to Unseen Domains: A Survey on Domain Generalization. *IEEE Transactions on Knowledge and Data Engineering* 35, 8 (2023), 8052–8072. <https://doi.org/10.1109/TKDE.2022.3178128>
- [54] Phillip Wenig, Sebastian Schmidl, and Thorsten Papenbrock. 2022. TimeEval: a benchmarking toolkit for time series anomaly detection algorithms. *Proc. VLDB Endow.* 15, 12 (Aug. 2022), 3678–3681. <https://doi.org/10.14778/3554821.3554873>
- [55] Haowen Xu, Wenxiao Chen, Nengwen Zhao, Zeyan Li, Jiahao Bu, Zhihan Li, Ying Liu, Youjian Zhao, Dan Pei, Yang Feng, Jie Chen, Zhaogang Wang, and Honglin Qiao. 2018. Unsupervised Anomaly Detection via Variational Auto-Encoder for Seasonal KPIs in Web Applications. In *Proceedings of the 2018 World Wide Web Conference (Lyon, France) (WWW '18)*. International World Wide Web Conferences Steering Committee, Republic and Canton of Geneva, CHE, 187–196. <https://doi.org/10.1145/3178876.3185996>
- [56] Yiyuan Yang, Chaoli Zhang, Tian Zhou, Qingsong Wen, and Liang Sun. 2023. DCdetector: Dual Attention Contrastive Representation Learning for Time Series Anomaly Detection. In *Proceedings of the 29th ACM SIGKDD Conference on Knowledge Discovery and Data Mining (Long Beach, CA, USA) (KDD '23)*. Association for Computing Machinery, New York, NY, USA, 3033–3045. <https://doi.org/10.1145/3580305.3599295>
- [57] Chuxu Zhang, Dongjin Song, Yuncong Chen, Xinyang Feng, Cristian Lumezanu, Wei Cheng, Jingchao Ni, Bo Zong, Haifeng Chen, and Nitesh V. Chawla. 2019. A deep neural network for unsupervised anomaly detection and diagnosis in multivariate time series data. In *Proceedings of the Thirty-Third AAAI Conference on Artificial Intelligence and Thirty-First Innovative Applications of Artificial Intelligence Conference and Ninth AAAI Symposium on Educational Advances in Artificial Intelligence (Honolulu, Hawaii, USA) (AAAI'19/IAAI'19/EAAI'19)*. AAAI Press, Article 174, 8 pages. <https://doi.org/10.1609/aaai.v33i01.33011409>
- [58] Zhenyu Zhong, Qiliang Fan, Jiacheng Zhang, Minghua Ma, Shenglin Zhang, Yongqian Sun, Qingwei Lin, Yuzhi Zhang, and Dan Pei. 2023. A Survey of Time Series Anomaly Detection Methods in the AIOps Domain. arXiv:2308.00393 [cs.LG]
- [59] Zhenyu Zhong, Qiliang Fan, Jiacheng Zhang, Minghua Ma, Shenglin Zhang, Yongqian Sun, Qingwei Lin, Yuzhi Zhang, and Dan Pei. 2023. A Survey of Time Series Anomaly Detection Methods in the AIOps Domain. arXiv:2308.00393 [cs.LG]
- [60] Kaiyang Zhou, Ziwei Liu, Yu Qiao, Tao Xiang, and Chen Change Loy. 2023. Domain Generalization: A Survey. *IEEE Trans. Pattern Anal. Mach. Intell.* 45, 4 (April 2023), 4396–4415. <https://doi.org/10.1109/TPAMI.2022.3195549>

A DETAILS ON THE EXPERIMENTAL SETUP

This section details the experimental setup we consider to run and evaluate AD methods on Exathlon’s dataset with respect to the problem statement of Section 4. This setup corresponds to the parameters we set for the corresponding steps (and substeps) of the Exathlon pipeline [25].

A.1 Data Selection

We never consider the Spark streaming applications 7 and 8, for which there are no disturbed and undisturbed traces, respectively. Our primary goal with this use case is to detect anomalies in the behavior of a running Spark streaming *application*, as opposed to the behavior of the entire four-node *cluster* an application is running on. As such, we always remove from our labels the CPU contention events that had no impact on a recorded application’s components (i.e., that occurred on nodes where this application had no running driver or executors). In practice, we label those anomalies the same way as other “*unknown*” anomalous events, in order not to penalize CPU contention Recall for missing them, nor Precision for detecting records as abnormal in these ranges.

A.2 Data Preprocessing

The metrics collected for Spark streaming traces allocated 140 columns for each of five “executor spots” in the data, saved in case one of the two to three active executors of an application failed during its execution. In practice, inactive executor spots in the data took the default value of -1 (as a placeholder for “null”). This value of -1 was however also (and mainly) used to refer to (a potential subset of) “missing” metrics, not received fast enough for the expected timestamp during data collection. This convention yielded two types of contiguous “ -1 ranges” for executor metrics in the data, with some meaning the executor was inactive, and some meaning it was not reachable by data collection (typically, but not only, during anomalies). For every executor e , we distinguish these two cases based on the `{e}_executor_runTime_count` counter metric. Specifically, if a -1 range occurs between two non- (-1) ranges and this counter metric was reset after it, then this -1 range corresponds to an “inactive executor range”. Otherwise, it corresponds to a “missing range”. We handle cases of starting and ending -1 ranges through a combination of manual inspection and duration rules. With these types of ranges distinguished, missing values were filled by propagating forward preceding valid values (or propagating backward following valid values when no such values existed). Inactive executor ranges were left as -1 .

After this preprocessing, all metrics in the data should be either positive or -1 . This was sometimes not the case for three specific metrics, which could mistakenly take the opposite of their “true value” due to other related metrics being -1 . For this reason, we also set all negative metrics different from -1 to their opposite values. Finally, to handle duplicate and missing timestamps, we resampled the data from all traces to match their supposed sampling period of one second (using the `max(·)` aggregation function).

A.3 Data Partitioning

This paper considers the setup of building a single AD method instance for all the Spark streaming applications in training, as opposed to building a distinct instance per application. We retained this setup to reduce the modeling cost as the number of applications increases. Besides, training a single model for a variety of entities is often considered more effective in practice, allowing this model to share knowledge across entities, and thus increasing data efficiency per entity [22]. We however do not require AD methods to generalize to *unseen* applications, by making sure the eight applications left after data selection are represented in both training and test.

We define our training sequences as most of the undisturbed traces, plus some disturbed traces to increase the variety in application *settings* and *input rates* for the methods to learn from. After data partitioning, our test sequences contain:

- 15 Bursty Input (T1) ranges.
- 5 Bursty Input Until Crash (T2) ranges.
- 6 Stalled Input (T3) ranges.
- 7 CPU Contention (T4) ranges.
- 5 Driver Failure (T5) ranges.
- 5 Executor Failure (T6) ranges.

A.4 Feature Engineering

All our compared methods consider the same features as input, built from an automated feature engineering step simply consisting in:

- Dropping the features collected by `nmon` (since these features reflect the behavior of the entire four-node cluster, sometimes unrelated to the application run represented in the trace).
- Dropping the features that were constant throughout the whole data.
- Differencing *cumulative* features (i.e., that were only increasing within a given trace).
- Averaging corresponding Spark executor features across “active executor spots” (non-(-1) after data preprocessing) into a single block of 140 features.

After this feature engineering, we get $M = 237$ features to use by the AD methods, which can be decomposed as follows:

- **168 Driver Features**
 - 18 “streaming” features. For example:
 - * The processing delay and scheduling delay of the last completed batch.
 - * The number of records in the last received batch.
 - 5 block manager features. For example:
 - * The disk space used by the block manager.
 - * The memory used by the block manager.
 - 32 JVM features. For example:
 - * The heap memory usage of the driver.
 - * The survivor space usage of the driver (the survivor space is a memory pool that holds objects having survived a young generation garbage collection, before those objects potentially get promoted to old generation memory).
 - 19 DAG scheduler features. For example:
 - * The number of active jobs.
 - * The number of running stages.
 - 94 live listener bus features. For example:
 - * The number of messages received from the DAG scheduler in the last 1, 5 and 15 minutes.
 - * The average processing time of messages received from the DAG scheduler.
- **69 Executor Features (Averaged Across Active Execs)**
 - 27 “executor” features. For example:
 - * The CPU time.
 - * The number of active tasks.
 - * The number of bytes read and written to HDFS.
 - 38 JVM features, similar to those of the driver.

- 4 netty block transfer features. For example:
 - * The direct memory used by the shuffle client and server of the netty network application framework (sending and receiving blocks of data).
 - * The heap memory used by the shuffle client and server of the netty network application framework.

A.5 Data Windowing

To compare different AD methods in a unified manner, this paper relies on the framework introduced in Section 3.2, only considering methods that are both trained and used on data windows, or *samples*, with anomaly scores derived from a window scoring function g_W . We therefore perform a data windowing step, producing sliding windows of length $L = 1$ for methods that model individual data records (called *point modeling* methods in the following), and $L = 20$ for *sequence modeling* methods.

Once sliding windows have been created from the training sequences, we *balance* them by according to their (application, Spark settings, input rate) triplet for the existing methods. Since there is no reason for AD methods to favor any particular values of those aspects, we indeed ensure every combination that exists in the training data is equally represented. For the DIVAD methods, we balance windows according to their *domain* instead. For both balancing strategies, we make sure this process preserves the data cardinality, by randomly undersampling the over-represented combinations, and randomly oversampling the under-represented ones.

A.6 AD Inference and Evaluation

When deriving our record scoring functions g , we always consider the following grid of anomaly score smoothing factors:

$$\gamma \in (0, 0.8, 0.9, 0.95, 0.96667, 0.975, 0.98, 0.98333, 0.9875, 0.99167, 0.99375, 0.995),$$

which corresponds to considering approximately the last:

$$n_\gamma \in (1, 5, 10, 20, 30, 40, 50, 60, 80, 120, 160, 200)$$

anomaly scores in the exponentially weighted moving average (with $n_\gamma = 1/(1 - \gamma)$).

In Exathlon, online scorers g are evaluated based on their ability to separate normal from anomalous records in anomaly score space, leaving the selection of a suitable threshold to human operators when the solution is deployed in practice [55]. A way to do so is by considering every possible detector f that can be derived from g using a fixed anomaly score threshold. That is, given the set of all anomaly scores g assigned in test sequences:

$$\hat{\mathcal{G}}_{\text{test}} := \bigcup_{i \in [N_1+1..N_1+N_2]} \left\{ \left\{ g(S^{(i)}; L, \gamma)_t, t \in [1..T] \right\} \right\},$$

consider all detectors $\mathcal{F} = \{f(\cdot; L, \gamma, \delta), \delta \in \hat{\mathcal{G}}_{\text{test}}\}$, where the binary record-wise prediction assigned by a detector $f(\cdot; L, \gamma, \delta)$ in a sequence S at time t is defined as:

$$f(S; L, \gamma, \delta)_t := g(S; L, \gamma)_t > \delta.$$

Plotting the Precision and Recall for every such detector on the test set gives the Precision-Recall (PR) curve. In this paper, we consider the Precision, Recall and F1-score achieved by the detector $f(\cdot; L, \gamma, \delta^*)$, where δ^* is the anomaly score threshold that gave the maximum F1-score on the test set (i.e., the “best” point on the PR-curve). We refer to this latter metric as the **peak F1-score** achieved by the online scorer g , indicating the detection performance this scorer would achieve given the adequate threshold. Like in [55], we indeed favor that AD methods induce a single, high-performing threshold over many “medium” ones. We consider *point-based* anomaly detection performance, and Recall values averaged across the different event types, deeming them equally important to detect no matter their cardinality in test data.

We benchmark AD methods assuming a purely unsupervised scenario, where labels are not assumed available even for tuning hyperparameters. As such, we report the performance of each method as its full box plot of peak F1-scores achieved across a “sensible” grid of hyperparameter values, like advised for instance in [2].

For every AD method, our window-based methodology to derive the record scoring function can induce “rightfully large” anomaly scores assigned to the $L - 1$ records immediately following an anomaly (since the windows of length L used to compute them are partially anomalous). This may introduce some rightful “lags” in the anomaly predictions, hindering the global performance despite the method behaving properly. We handle this aspect by ignoring the $L - 1$ records following each test anomaly in our evaluation, where L is the window length used by the AD method.

B DETAILS ON THE EXISTING METHODS

This section provides details about the existing methods compared, covering the model training and selection strategy we used for deep learning methods, as well as a short description and the hyperparameter grid considered for each method.

B.1 Model Training and Selection for Deep Learning Methods

All of the deep learning methods considered used the same random 20% of training data as validation, sampled in a stratified manner with traces as strata, with the labeled training and validation anomalies removed. Unless mentioned otherwise, all deep learning methods were trained with a Stochastic Gradient Descent (SGD) strategy, using mini-batches of size B , the AdamW optimizer [32], and a weight decay coefficient of 0.01. For all methods and sets of hyperparameters, we considered a grid of learning rate values $\eta \in \{1e-5, 3e-5, 1e-4, 3e-4\}$, and selected the learning rate that yielded the lowest validation loss (i.e., the best *modeling* performance, like in [6]). All methods were trained for 300 epochs by default, using early stopping and checkpointing on the validation loss with a patience of 100 epochs.

B.2 Point Modeling Methods

Point modeling methods model individual data records ($L = 1$), assumed independent and identically distributed (i.i.d). As such, they only rely on our feature engineering and anomaly score smoothing to capture the sequential aspect of the data. We include the following point modeling methods in our study:

- Isolation forest [31] (**iForest**) as an isolation tree method.
- Principal Component Analysis (**PCA**) [47] and Dense Autoencoder (**Dense AE**) [21, 44] as reconstruction methods.
- Dense Deep SVDD [42] (**Dense DSVDD**) as an encoding method.
- Mahalanobis [3, 47] (**Maha**) and Dense Variational Autoencoder (**Dense VAE**) [7] as distribution methods.

Isolation forest trains an ensemble of trees to isolate the samples in the training data, and defines the anomaly score of a test instance proportionally to the average path length required to reach it using the trees. We report its performance with the following hyperparameters (using the default values of Scikit-Learn 1.0.2 [36] for the ones not mentioned):

- A number of trees in $\{50, 100, 200, 500, 1000\}$.
- A maximum number of samples used by each tree in $\{256, 512, 2048, 8192, 32768\}$.
- A maximum number of features used by each tree of 64.

As reconstruction methods, PCA and Dense AE define anomaly scores of test vectors as their mean squared reconstruction errors from a transformed (latent) space. The transformation of PCA is a projection on the linear hyperplane formed by the principal components of the data. We report its performance with the following preprocessing and hyperparameters (using the default values of Scikit-Learn 1.0.2 for the ones not mentioned):

- A standardization of the input samples.
- A number of principal components (latent dimension) in $\{16, 64, 128, 95\%, 99\%, M\}$, where 95% and 99% correspond to the latent dimension preserving 95% and 99% of the training data variance, respectively, and $M = 237$ is our input dimensionality after feature engineering.

The transformation of the Autoencoder method is a non-linear mapping to a latent encoding learned by a neural network that was trained to reconstruct input data from it. With Dense AE, we consider a fully-connected architecture for this neural network, and report its performance with the following preprocessing and hyperparameters:

- A standardization of the input samples.
- A single hidden layer of 200 units for both the encoder and the decoder.
- The Rectified Linear Unit (ReLU) activation function for all the layers except the output, for which we do not use any activation function.
- An encoding dimension in $\{16, 64\}$.
- A batch size $B = 32$.

The Mahalanobis and VAE methods define anomaly scores of data samples as their deviation from an estimated data distribution. The Mahalanobis method estimates this distribution as a multivariate Gaussian, and defines the anomaly score of a test vector as its squared Mahalanobis distance from it. As such, it does not require any hyperparameters, and we therefore report its performance using only a standardization of the input samples. Dense VAE estimates the data distribution using a fully-connected variational autoencoder, with the anomaly score of a test point derived by drawing multiple samples from the probabilistic encoder, and averaging the negative log-likelihood of the reconstructions obtained

from each of these samples. We report its performance using the following preprocessing and hyperparameters:

- A standardization of the input samples.
- A single hidden layer of 200 units for both the encoder and the decoder.
- An encoding dimension in $\{16, 64\}$.
- The ReLU activation function for all the layers except the encoding and output. To improve numerical stability, we adopt a similar strategy to Xu et al. [55], and derive the standard deviations of encodings and outputs using softplus activations shifted by a small constant ϵ set to $1e-4$.
- A batch size $B = 32$.
- A number of samples drawn of 256 to derive the anomaly score of a test example.

The Dense DSVDD method trains a fully-connected neural network to map the input data to a latent representation enclosed in a small hypersphere, and then defines anomaly scores of test samples as their squared distance from this hypersphere’s centroid. We use the implementation of Ruff et al. [43] with the “One-Class Deep SVDD” objective (assuming most of the training data is normal) and their initialization of the encoder weights from a pretrained autoencoder model. We report the performance of Dense DSVDD with the following preprocessing and hyperparameters (using the same values as the original implementation for those not mentioned):

- A standardization of the input samples (we also tried the original paper’s strategy of normalizing the inputs and using a sigmoid activation function for the output layer, but this did not lead to a better performance).
- A single hidden layer of 200 units for the encoder and the decoder (with the decoder only being used for pretraining).
- An encoding dimension in $\{16, 64\}$.
- The Leaky ReLU activation function with a negative slope coefficient $\alpha = 0.01$ for all the layers except the encoding and decoder output (like in the original implementation).
- A batch size $B = 200$ (like in the original implementation).
- A pretraining phase of 150 epochs, followed by a training phase of 150 epochs (which makes the same total number of 300 epochs as the other methods).
- The same learning rate and optimization strategy for the pretraining and training phases.
- The same grid of learning rate values as the other methods, but dividing the learning rate by 10 after 50 epochs (like in the original implementation). Larger learning rate values were also tried due to this scheduling, but did not produce better results.
- A weight decay coefficient of $1e-6$ (like in the original implementation).

B.3 Sequence Modeling Methods

Sequence modeling methods model wider *windows* of data records ($L = 20$ here), which offers them the capacity of explicitly considering the temporal aspect of the data. We include the following sequence modeling methods in our study:

- Recurrent Autoencoder [21, 44] (**Rec AE**), **MSCRED** [57] and **TranAD** [50], as the sequence modeling version of

Dense AE and more recent reconstruction methods, respectively.

- **LSTM-AD** [34], as the most popular forecasting method.
- Recurrent Deep SVDD [42] (**Rec DSVDD**) as the sequence modeling version of the Dense DSVDD encoding method.
- Recurrent VAE (**Rec VAE**) and OmniAnomaly [48] (**Omni**) as the sequence modeling version of Dense VAE and a more recent distribution method, respectively.

Rec AE uses the same modeling and scoring strategy as Dense AE, with the fully-connected neural network architecture replaced by a recurrent one. Figure 16 illustrates the general form we adopted for our recurrent autoencoders, including 1D convolutional and recurrent layers. In this design, the encoder first consists of an optional stack of 1D convolutional layers, which in this example contains a single layer labeled $\text{Conv1D}(32, 5, s)$, to indicate it has 32 filters of size 5 and a stride length hyperparameter s . These layers result in a new latent window length $L' \leq L$ for an input window, with one feature map per filter in the last layer. These feature maps get sent to an optional stack of GRU layers, here shown as a single layer labeled $\text{GRU}(64, \text{Last})$, to indicate it has 64 units and returns its outputs for the last time step only. These layers are followed by a fully-connected layer that outputs the final encoding. This encoding is provided as input to the decoder, which repeats it L' times to match the window length of the data after the 1D convolutions. This repeated vector goes through a stack of GRU layers typically defined symmetrically to the encoder’s, except it now returns its outputs for each of the L' time steps. These outputs finally get passed to a stack of 1D transposed convolutional layers defined symmetrically to the encoder’s 1D convolutional layer stack, except for the output layer using M filters to match the input dimensionality. We report the performance of Rec AE using the following preprocessing and hyperparameters:

- A standardization of the input samples.
- An encoder with a 1D convolutional layer using 32 filters of size 5, a stride length of 1 and the ReLU activation function, followed by a GRU layer of 64 units using the hyperbolic tangent (\tanh) activation function, and a fully-connected layer to output the encoding.
- A decoder defined symmetrically to the encoder as per the design of Figure 16.
- An encoding dimension in $\{64, 128\}$, with the ReLU activation function for the encoding layer.
- A batch size $B = 32$.

TranAD uses a transformer-based model with self-conditioning, an adversarial training procedure and model-agnostic meta learning (MAML). It relies on two encoder-decoder networks, with the first encoder considering the current input window, and the second one considering a larger *context* of past data in the window’s sequence. The method defines the anomaly score of an input window as the average of its reconstruction errors coming from two decoders and inference phases, with the second phase using the reconstruction error from the first phase as a focus score to detect anomalies at a finer level. Compared to the other methods, TranAD therefore considers training windows augmented with their past sequence data, which prevented us from applying our simple window balancing strategy. We report the performance of TranAD using the

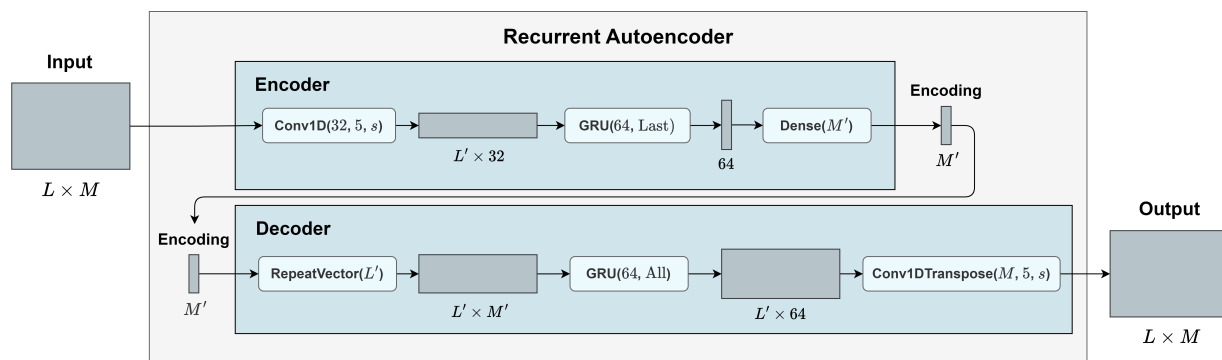


Figure 16: General form of our recurrent autoencoder architectures.

implementation of Tuli et al. [50], only specifying manually the following preprocessing and hyperparameters:

- A normalization of the input samples (like in the original implementation). We also tried the strategy of standardizing the inputs and using no activation function for the output layer (like the other methods), but this did not lead to a better performance.
- A number of encoder hidden units in $\{64, 128\}$.
- The same grid of learning rate values as the other methods, but multiplying the learning rate by 0.9 every 5 epochs (like in the original implementation). Larger learning rate values were also tried due to this scheduling, but did not produce better results.
- A batch size $B = 128$ (like in the original implementation).
- A weight decay coefficient of $1e-5$ (like in the original implementation).

MSCRED turns a multivariate time series into multi-scale signature matrices characterizing system status at different time steps, and learns to reconstruct them using convolutional encoder-decoder and attention-based ConvLSTM networks. We report the performance of MSCRED using the implementation from TimeEval [54], only specifying manually the following preprocessing and hyperparameters:

- A standardization of the input samples.
- Two signature matrices of lengths $w = 5, 10$ at each time step, with no gap between consecutive computations.
- A number of convolutional encoder layers in $\{2, 3\}$, of the form $((32, 8, 8), (128, 8, 8))$ in case of 2 layers, and $((32, 8, 8), (64, 4, 4), (128, 4, 2))$ in case of 3 layers, with (f, k, s) the number of filters, filter size and stride length of a layer, respectively.
- The attention-based ConvLSTM and convolutional decoder networks derived from the convolutional encoder like in the original implementation.
- A batch size $B = 64$.
- A number of epochs of 20, with an early stopping patience of 10 epochs.

LSTM-AD trains a stacked LSTM network to predict the next l data records from the first $L - l$ of a window. Originally designed for univariate time series, this method produces an l -dimensional

vector of forecasting errors for each data record in a test sequence, with one component for each position held by this record in forecast windows of length l . The method then fits a multivariate Gaussian distribution to the error vectors it produced in a validation set, and defines the anomaly score of a test record as the negative log-likelihood of its error with respect to this distribution. In this work, we adapt LSTM-AD to multivariate data by considering the $l \times M$ matrix of forecasting errors made for a data record at each time step and feature, and averaging these errors across the feature dimension to get the l -dimensional vector of the original method. We report the performance of LSTM-AD using the following hyperparameters:

- A standardization of the input samples.
- A forecast window length $l = 10$ (i.e., half of our window length $L = 20$).
- A version with a single LSTM layer of 128 units, and a version with two LSTM layers of 128 units each, all using the tanh activation function.
- A batch size $B = 32$.

Rec DSVDD uses the same modeling and scoring strategy as Dense DSVDD, with the fully-connected neural network architecture replaced by a recurrent one, adapting the implementation of Ruff et al. [43] to match the design of Figure 16. We report the performance of Rec DSVDD with the following preprocessing and hyperparameters (using the same values as the original implementation for those not mentioned):

- A standardization of the input samples.
- An encoder with a 1D convolutional layer using 32 filters of size 5, a stride length of 1, batch normalization and the Leaky ReLU activation function (with a negative slope coefficient $\alpha = 0.01$), followed by a GRU layer of 64 units and a fully-connected layer to output the encoding.
- A pretraining decoder defined symmetrically to the encoder as per the design of Figure 16.
- An encoding dimension in $\{64, 128\}$, with no activation function for the encoding layer.
- A batch size $B = 200$ (like in the original implementation).
- A pretraining phase of 150 epochs, followed by a training phase of 150 epochs.
- The same learning rate and optimization strategy for the pretraining and training phases.

- The same grid of learning rate values as the other methods, but dividing the learning rate by 10 after 50 epochs (like in the original implementation).
- A weight decay coefficient of $1e-6$ (like in the original implementation).

Rec VAE uses the same modeling and scoring strategy as Dense VAE, with the fully-connected neural network architecture replaced by a recurrent one following the design of Figure 16. We report the performance of Rec VAE using the following preprocessing and hyperparameters:

- A standardization of the input samples.
- An encoder with a 1D convolutional layer using 32 filters of size 5, a stride length of 1 and the ReLU activation function, followed by a GRU layer of 64 units using the tanh activation function, and a fully-connected layer to output the encoding parameters.
- A decoder defined symmetrically to the encoder as per the design of Figure 16.
- An encoding dimension in $\{64, 128\}$.
- The same strategy as Dense VAE for deriving the encoding and output standard deviations.
- A batch size $B = 32$.
- A number of samples drawn of 256 to derive the anomaly score of a test example.

OmniAnomaly [48] estimates the distribution of multivariate windows with a stochastic recurrent neural network, explicitly modeling temporal dependencies among variables through a combination of GRU and VAE. It then defines a test window’s anomaly score as the negative log-likelihood of its reconstruction. We report the performance of OmniAnomaly using the implementation of Su et al. [48], only specifying manually the following preprocessing and hyperparameters:

- A normalization of the input samples (like in the original implementation). We also tried the strategy of standardizing the inputs (like the other methods), but this did not lead to a better performance.
- A number of units of 200 for the fully-connected and GRU layers.
- A number of planar normalizing flow layers of 10.
- An encoding dimension in $\{64, 128\}$.
- An L2 regularization coefficient of $1e-4$ for all layers (like in the original implementation).
- A batch size $B = 64$.
- The Adam optimizer with a grid $\{3e-5, 1e-4, 3e-4, 1e-3\}$ for the initial learning rate, dividing the learning rate by 2 every 20 epochs.
- A gradient norm limit of 10.0 (like in the original implementation).
- A number of epochs of 40, with an early stopping patience of 10 validations. To accelerate computations, we run validation 5 times per epoch, instead of once every 100 steps in the original implementation.

C DETAILS ON THE DIVAD VARIANTS

This section provides details about our DIVAD variants, covering our model training and selection strategy, as well as the architecture and hyperparameter grid considered for each variant.

We adopt the same model training and selection strategy as described in Appendix B.1 for both DIVAD-G and DIVAD-GM. Like for DIVA [24], we do not share the parameters of our encoder networks NN_{ϕ_y} and NN_{ϕ_d} , but consider the *multi-encoder* architecture illustrated in Figure 4. For both variants, we use the same strategy as Dense VAE and Rec VAE for deriving encoding and output standard deviations.

We first consider *point modeling* DIVAD variants ($L = 1$), using fully-connected neural network architectures and referred to as **Dense DIVAD-G** and **Dense DIVAD-GM**, respectively. We report the performance of Dense DIVAD-G using the following preprocessing and hyperparameters:

- A standardization of the input samples.
- A single hidden layer of 200 units for the encoders NN_{ϕ_y} and NN_{ϕ_d} as well as for the decoder $NN_{\theta_{yd}}$.
- A single fully-connected hidden layer of 64 units for the conditional domain prior network NN_{θ_d} .
- A ReLU activation function followed by a single fully-connected layer of $N_{\text{dom}} = 22$ units (i.e., one per source domain) for the classification head NN_{ω_d} . The domain encoding z_d is indeed sampled unbounded from $q_{\phi_d}(z_d|x)$, so we pass it through a ReLU activation before applying the output layer. The classification head was intentionally kept simple, so as to be able to *easily* classify the domain from z_d .
- The ReLU activation function for all the layers except the encoding and output layers.
- An encoding dimension in $\{16, 64\}$.
- A KL divergence weight $\beta \in \{1, 5\}$.
- A domain classification weight $\alpha_d = 100,000$. We set this weight based on the scale we observed for our losses $\mathcal{L}_{\text{ELBO}}$ and \mathcal{L}_d during training in some initial experiments. We also tried the CoV-Weighting strategy proposed by Groenendijk et al. [18] to automatically balance these two losses, but this did not lead to a better performance.
- A batch size $B = 128$.
- An anomaly scoring based on the class encoding aggregated posterior estimate $\hat{q}_{\phi_y}(z_y)$, fitting a multivariate Gaussian distribution to the training class encodings.

We report the performance of Dense DIVAD-GM using the following preprocessing and hyperparameters:

- A standardization of the input samples.
- The same architectures as Dense DIVAD-G for the networks NN_{ϕ_y} , NN_{ϕ_d} , $NN_{\theta_{yd}}$, NN_{θ_d} and NN_{ω_d} .
- An encoding dimension in $\{16, 32\}$, with $K = 8$ Gaussian Mixture components when using an encoding dimension of 16, and $K = 4$ components when using an encoding dimension of 32.
- A KL divergence weight $\beta \in \{1, 5\}$.
- A domain classification weight $\alpha_d = 100,000$.
- A batch size $B = 128$.

- An anomaly scoring based on (i) the learned class encoding prior $p_\lambda(\mathbf{z}_y)$, and (ii) the class encoding aggregated posterior estimate $\hat{q}_{\phi_y}(\mathbf{z}_y)$, fitting a Gaussian Mixture distribution with K components to the training class encodings.

We also consider *sequence modeling* DIVAD variants ($L = 20$ here), with some fully-connected neural network architectures replaced by recurrent ones based on the design of Figure 16, referred to as **Rec DIVAD-G** and **Rec DIVAD-GM**, respectively. We report the performance of Rec DIVAD-G using the following preprocessing and hyperparameters:

- A standardization of the input samples.
- Each encoder NN_{ϕ_y} and NN_{ϕ_d} with a 1D convolutional layer using 64 filters of size 5, a stride length of 1 and the ReLU activation function, followed by a GRU layer of 64 units using the tanh activation function, and a fully-connected layer to output the encoding parameters.
- The decoder $\text{NN}_{\theta_{yd}}$ defined symmetrically to one encoder as per the design of Figure 16.
- The same architectures as Dense DIVAD-G for the conditional domain prior network NN_{θ_d} and classification head NN_{ω_d} .
- An encoding dimension of 32.
- A KL divergence weight $\beta \in \{1, 5\}$.
- A domain classification weight $\alpha_d = 100,000$.
- A batch size $B = 128$.
- The same anomaly scoring as Dense DIVAD-G.

We report the performance of Rec DIVAD-GM using the following preprocessing and hyperparameters:

- A standardization of the input samples.
- The same architectures as Rec DIVAD-G for the networks NN_{ϕ_y} , NN_{ϕ_d} , $\text{NN}_{\theta_{yd}}$, NN_{θ_d} and NN_{ω_d} .
- An encoding dimension of 32, with $K = 8$ Gaussian Mixture components.
- A KL divergence weight $\beta \in \{1, 5\}$.
- A domain classification weight $\alpha_d = 100,000$.
- A batch size $B = 128$.
- The same anomaly scoring as Dense DIVAD-GM.

D ADDITIONAL ANALYSES ON EXATHLON

This section provides additional analyses of the results obtained using the Exathlon benchmark.

The lower performance observed for sequence modeling DIVAD variants could be explained by the *heightened challenge of learning domain-invariant patterns in the sequential setting*. While leveraging sequential information can be useful in theory, identifying domain-invariant *shapes* within and across $M = 237$ time series constitutes a harder task than relying on simple feature combinations at given time steps for our dataset and setup. This is illustrated in Figure 17, showing KDE plots of Rec DIVAD-GM’s anomaly scores for training normal, test normal and test anomalous records. From this figure, we can see that the domain generalization performed by Rec DIVAD-GM was less effective than for Dense DIVAD-GM and Rec DIVAD-G (see Figures 8 and 18, respectively), with its anomaly scores *drifting* from the training to the test normal records (**green** vs. **blue** KDEs). This suboptimal domain generalization led to a higher overlap

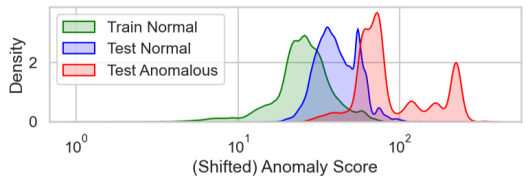


Figure 17: KDE plots of the anomaly scores assigned by Rec DIVAD-GM to training normal, test normal, and test anomalous records.

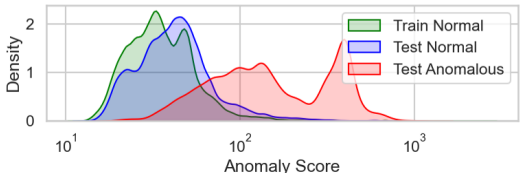


Figure 18: KDE plots of the anomaly scores assigned by Rec DIVAD-G to training normal, test normal, and test anomalous records.

between the anomaly scores of the test normal and anomalous records (**blue** vs. **red** KDEs), explaining the lower performance.

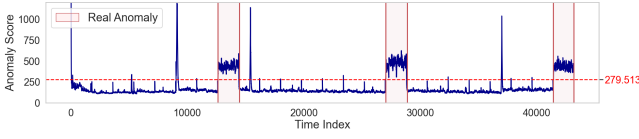
It is worth noting that the low performance of sequence modeling variants can also be explained by the *unsupervised nature* of our DIVAD methods, resulting in a lack of incentive for them to learn domain-invariant patterns that are sure to preserve anomaly signals. With point modeling, the feature combinations that tended to be domain-invariant were also useful to detect the anomalies of our dataset and setup. For Rec DIVAD-G, however, the *sequential* patterns learned to be shared across domains also tended to be shared between normal data and specific anomaly types. As illustrated in Figure 18, showing KDE plots of the anomaly scores assigned by Rec DIVAD-G to training normal, test normal and test anomalous records, Rec DIVAD-G could accurately perform its DG task, with training and test normal records getting assigned similar anomaly scores (aligned **green** and **blue** KDEs). This accurate DG however did not result in a better performance, due to Rec DIVAD-G’s inability to distinguish some anomalous records from normal data in domain-invariant space (high **blue** and **red** KDEs overlap). Figure 19, showing time plots of the anomaly scores assigned by Dense DIVAD-G and Rec DIVAD-G in trace 5_1_100000_63 (Bursty Input), further illustrates this for T1 events specifically. From these figures, we can see that, while Dense DIVAD-G accurately deemed T1 records “more abnormal” than most normal records in the trace, the encoding performed by Rec DIVAD-G tended to *remove* most of the anomalous signals from these events.

E DETAILS ON TIME MEASUREMENTS

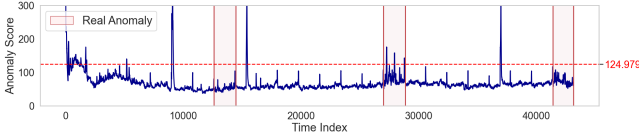
This section provides details about the time measurements we performed for the VAE and DIVAD variants.

Table 1 shows the average training and inference step times for the VAE and DIVAD variants on an NVIDIA A100 80GB PCIe, computed across the first 1000 mini-batches of size $B = 32$ (skipping the very first ones), with hyperparameters adjusted so as to make DIVAD and VAE directly comparable. Specifically, we ran:

- All methods with an encoding dimension of 16.



(a) Dense DIVAD-G.



(b) Rec DIVAD-G.

Figure 19: Time plots of the anomaly scores of Dense DIVAD-G and Rec DIVAD-G for the records in trace 5_1_100000_63 (Bursty Input), highlighting their peak F1-score thresholds and the ground-truth anomaly ranges.

- Dense VAE, Dense DIVAD-G and Dense DIVAD-GM using a single hidden layer of 200 units for the encoder and decoder networks.
- Rec VAE, Rec DIVAD-G and Rec DIVAD-GM using encoders with a 1D convolutional layer of 32 filters of size 5 and a stride length of 1, followed by a GRU layer of 64 units, and decoders defined symmetrically as per the design of Figure 16.
- The anomaly scoring of VAE redefined to consider the variational posterior’s *mean* instead of 256 samples, so as to match DIVAD’s anomaly scoring strategy.
- The anomaly scoring of DIVAD based on the class encoding prior $p_{\lambda}(z_y)$. Considering scoring from the aggregated posterior estimate indeed makes negligible differences at inference time, only attributable to the tool used to separately model the distribution.

We set the rest of VAE and DIVAD’s hyperparameters as described in Appendices B and C, respectively. Both VAE and DIVAD were implemented using TensorFlow 2.14.0 [1] and TensorFlow Probability 0.22.1 [12].

F DETAILS ON THE ASD EXPERIMENT

This section provides details about the experiment we conducted on the Application Server Dataset (ASD) [30].

We report the performance of TranAD using the implementation of Tuli et al. [50], and the same preprocessing and hyperparameters as for the Spark streaming dataset. For Rec DIVAD-GM, we consider each server trace as a separate *domain*, and report its performance using the following preprocessing and hyperparameters:

- A standardization of the input samples.
- Each encoder NN_{ϕ_y} and NN_{ϕ_d} with a 1D convolutional layer using 32 filters of size 5, a stride length of 1 and the ReLU activation function, followed by a GRU layer of 32 units using the tanh activation function, and a fully-connected layer to output the encoding parameters.
- The decoder $NN_{\theta_{yd}}$ defined symmetrically to one encoder as per the design of Figure 16.
- A single fully-connected hidden layer of 32 units for the conditional domain prior network NN_{θ_d} .
- A ReLU activation function followed by a single fully-connected layer of $N_{\text{dom}} = 11$ units (i.e., one per source domain) for the classification head NN_{ω_d} .
- An encoding dimension of 16, with $K = 8$ Gaussian Mixture components.
- A KL divergence weight $\beta \in \{1, 5\}$.
- A domain classification weight $\alpha_d = 1, 000$.
- A batch size $B = 128$.
- An anomaly scoring based on the class encoding aggregated posterior estimate $\hat{q}_{\phi_y}(z_y)$, fitting a Gaussian Mixture distribution with $K = 8$ components to the training class encodings.